Biomaterials 129 (2017) 83–97

Contents lists available at ScienceDirect

Biomaterials

journal homepage: www.elsevier.com/locate/biomaterials

Lanthanide-integrated supramolecular polymeric nanoassembly with multiple regulation characteristics for multidrug-resistant cancer therapy

Weihong Jin [a, 1], Qiwen Wang [b, c, 1], Min Wu [a, b], Yang Li [a, b], Guping Tang [a, b, ***], Yuan Ping [d, **], Paul K. Chu [a, *]

[a] Department of Physics and Materials Science, City University of Hong Kong, Tat Chee Avenue, Kowloon, Hong Kong, China
[b] Institute of Chemical Biology and Pharmaceutical Chemistry, Zhejiang University, Hangzhou, 310028, China
[c] Department of Cardiology, The First Affiliated Hospital, Zhejiang University School of Medicine, Hangzhou, 310003, China
[d] School of Materials Science and Engineering, Nanyang Technological University, Singapore, 639798, Singapore

ARTICLE INFO

Article history:
Received 18 December 2016
Received in revised form
12 March 2017
Accepted 13 March 2017
Available online 16 March 2017

Keywords:
Nanomedicine
Organic-inorganic hybrid materials
siRNA
Drug delivery
Chemotherapy

ABSTRACT

Cancer treatment can in principle be enhanced by the synergistic effects of chemo- and nucleic acid-based combination therapies but the lack of efficient drug nanocarriers and occurrence of multidrug resistance (MDR) are major obstacles adversely affecting the effectiveness. Herein, a lanthanide-integrated supramolecular polymeric nanoassembly that delivers anticancer drugs and siRNA for more effective cancer therapy is described. This nanotherapeutic system is prepared by loading adamantane-modified doxorubicin (Dox) into polyethylenimine-crosslinked-γ-cyclodextrin (PC) through the supramolecular assembly to form the interior Dox-loaded PC (PCD) followed by electrostatically driven self-assembly of siRNA and PCD to produce the PCD/siRNA nanocomplexes. The PCD/siRNA nanocomplex is further decorated with the exterior neodymium (Nd)-integrated PC (Nd-PC) layer to obtain the PCD/siRNA/Nd-PC nanoassembly in which the interior PC serves as an efficient carrier for simultaneous delivery of Dox and siRNA to the human breast cancer cell line, Dox-resistant MCF-7 (MCF-7/ADR) both *in vitro* and *in vivo*. The exterior Nd-PC layer improves the drug sensitivity to the MCF-7/ADR cells as a result of the improved nanoassembly uptake, reduced drug efflux, and enhanced apoptosis, as evidenced by multiple regulation of a series of intracellular proteins related to MDR. Furthermore, *in vivo* delivery of the PCD/siRNA/Nd-PC nanoassembly is demonstrated to inhibit tumor growth in the mouse model with MCF-7/ADR tumor xenografts as a result of reduced angiogenesis and increased necrosis at the tumor site. This study reveals a simple and universal strategy to transform polymer-based nanoassemblies into advanced organic-inorganic nanotherapeutics suitable for cancer MDR therapy.

1. Introduction

Cancer is a complex disorder resulting from multiple genetic changes as well as cellular abnormalities and treatment can be difficult. In chemotherapies, cancer cells often develop resistance to multiple drugs with different chemical structures and mechanisms. The phenomenon, known as multidrug resistance (MDR), represents one of the major hurdles in cancer chemotherapy and contributes to the failure in the treatment of metastatic cancer [1]. Owing to the complexity of MDR, combination therapies involving two or more therapeutic drugs with different mechanisms have gained more attention recently [2]. Several drug delivery strategies have been proposed to overcome MDR and one of the promising approaches is to incorporate both chemotherapeutics and MDR modulators into nanoparticles to produce synergetic effects. For example, liposomes loaded with the cytotoxic drug and efflux pump are more cytotoxic to cancer cells than the free drug or nanoparticles loaded only with drugs [3,4]. Therefore, co-delivery of chemotherapeutics and MDR inhibitors can effectively suppress tumor cell growth and invasion by reversing the

* Corresponding author.
** Corresponding author.
*** Corresponding author. Department of Physics and Materials Science, City University of Hong Kong, Tat Chee Avenue, Kowloon, Hong Kong, China.
E-mail addresses: tangguping@zju.edu.cn (G. Tang), pingyuan7@gmail.com (Y. Ping), paul.chu@cityu.edu.hk (P.K. Chu).
[1] Both authors contributed equally to this work.

http://dx.doi.org/10.1016/j.biomaterials.2017.03.020
0142-9612/

chemotherapeutic sensitivity [5,6]. Recently, RNA interference (RNAi) strategies to inhibit efflux pumps have been explored by exploiting siRNA as an alternative MDR modulator [7]. Despite the prospect of combination therapies, the therapeutic effect of co-delivery systems is restricted due to the lack of promising delivery vectors and hence, development of a functional delivery vehicle to maximize the effectiveness of combination therapies is needed.

Metal-incorporated organic assemblies combine the virtues of organic and inorganic materials to produce synergistic effects in biological applications [8–10]. For instance, surface functionalization of polymeric nanomaterials by plasma-based metal ion implantation has been applied to artificial blood vessels and antibacterial materials [11–13]. Metals such lanthanides, which are essential elements in the body, maintain the functionalities of proteins and enzymes and are involved in many physiological processes such as metabolism regulation, cell function promotion, and immune system maintenance [14,15]. Lanthanides can be transported into cells through the calcium ion channels or sodium-calcium exchange pathway [16–18] and the ability of lanthanides to activate endocytosis in plant cells has been demonstrated recently [19]. Lanthanides can facilitate cellular uptake of certain drugs by increasing the cell permeability [20,21] and suppress proliferation of cancer cells, as manifested by the decreased calmodulin (CaM) expression as well as up-regulation of other gene expressions in cancer cells [22]. Last but not least, lanthanides can induce significant morphological changes, arrest the transition from G0/G1 to S state [23], and trigger the receptor-mediated extrinsic pathway of apoptosis [24]. Our recent study on the neodymium (Nd)-functionalized gene delivery vector reveals higher gene transfection activity by stimulation of the cellular energy metabolism and enhancement of cellular uptake ability [25]. We have also demonstrated that supramolecular cationic polyethyleneimine (PEI)-cyclodextrin conjugates are efficient carriers to encapsulate hydrophilic drugs *via* host-guest interactions and induce nucleic acid complexation by electrostatic interaction [26,27].

In this work, we design and prepare a lanthanide-integrated supramolecular nanoassembly serving as an efficient carrier for simultaneous delivery of chemotherapeutic drugs and siRNA to combat cancer MDR (Fig. 1). Doxorubicin (Dox) is first conjugated with 1-adamantanecarboxylic acid (Ada-COOH) to form adamantane-modified doxorubicin (Ada-Dox). Ada-Dox is then incorporated into the hydrophobic cavities of (2-hydroxypropyl)-γ-cyclodextrins (HP-CD) on polyethylenimine-crosslinked γ-cyclodextrins (PC) *via* host-guest interactions between the adamantyl group and cyclodextrin to form Dox-loaded PC (PCD) as a core with positive surface charges. Negatively charged siRNA is then wrapped onto the exofacial surface of the PCD core by interacting with cationic polyethyleneimine arms to form the PCD/siRNA complexes. Finally, lanthanide integration is achieved by decorating the PCD/siRNA complexes with Nd-doped PC (Nd-PC) to form the PCD/siRNA/Nd-PC tertiary nanoassembly. The Nd-PC in the outer layer of the PCD/siRNA/Nd-PC nanoassembly provides a protective layer to prevent the siRNA from degradation in the bloodstream and interacts with the cell membrane to enhance penetration of the PCD/siRNA/Nd-PC nanoassembly through either the clathrin-mediated or caveolin-mediated endocytosis. Since the outer Nd-PC layer contains a large number of secondary and tertiary amines, protonation of the amino groups after cellular endocytosis causes accumulation of protons leading to influx of counter ions causing swelling and disruption of the endosome that traps the PCD/siRNA/Nd-PC nanoassembly. In the meantime, the release of siRNA is induced by the competitive interaction of the negatively charged substances in the cytoplasm [28,29] and Ada-Dox may be detached from the cavity of CD in PCD followed by the release of Dox under acidic and enzymatic conditions. The released siRNA into the cytoplasm down-regulates the P-gp protein expression, turns off the P-gp pump, and retards the efflux of the released Dox. This greatly facilitates the release Dox preserved in the cells and allows Dox to diffuse passively into nuclei to produce high cancer cell killing efficacy. The *in vitro* and *in vivo* therapeutic effects are investigated in terms of cellular uptake, cell apoptosis, tumor weight and volume, tumor angiogenesis, as well as immunohistology of tumor slices. Regulation of a series of proteins is also

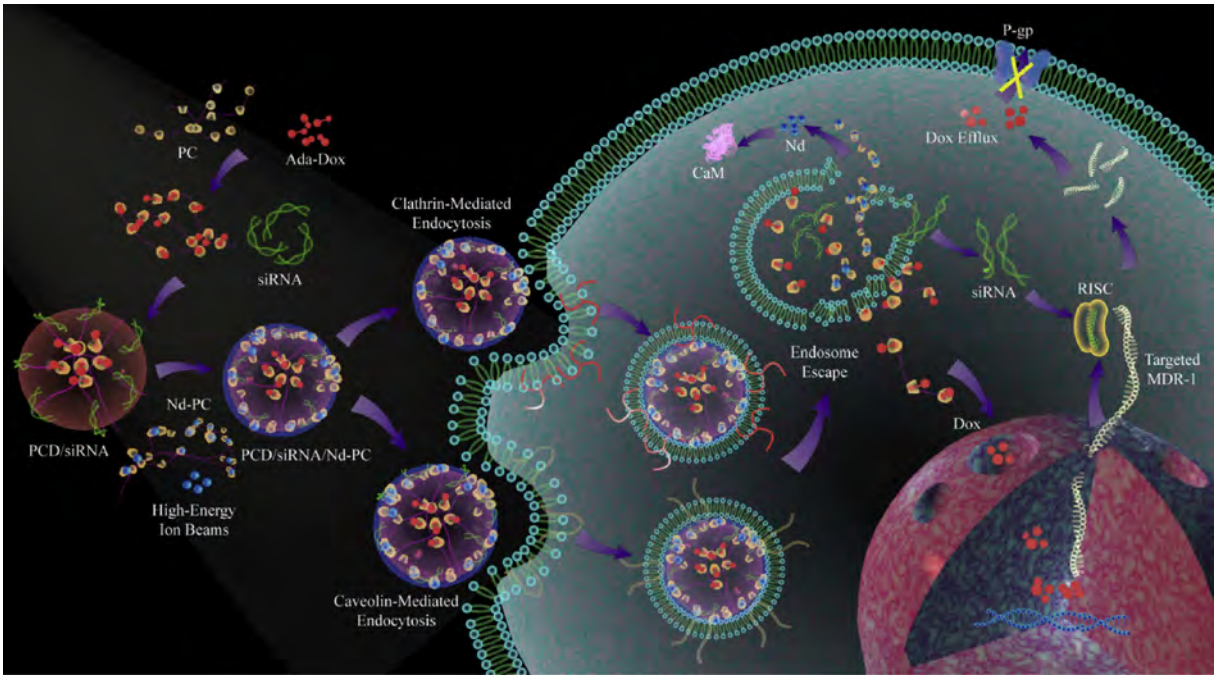

Fig. 1. Schematic illustration of the fabrication of the PCD/siRNA/Nd-PC nanoassembly and intracellular delivery mediated by the PCD/siRNA/Nd-PC nanoassembly.

examined *in vitro* and *in vivo* after administration of the Nd-integrated supramolecular polymeric nanoassembly. To the best of our knowledge, this is the first demonstration of successful reversal of tumor MDR by delivery of a lanthanide-integrated polymeric nanoassembly and our findings disclose the possibility of lanthanide-integrated polymeric therapeutics in treating various types of MDR cases.

2. Materials and methods

2.1. Materials

Branched PEI (MW 600 Da), γ-cyclodextrin (CD) (MW 1297), 1,10-carbonyldiimidazole (CDI, MW 162.15), triethylamine (99%), dimethyl sulfoxide (DMSO, ≥99.5%), and [3-(4,5-dimethylthiazol-2-yl)-2,5-diphenyltetrazolium bromide] (MTT, 98%) were purchased from Sigma-Aldrich (St. Louis, MO, USA). Dox hydrochloride (MW 543.52) was obtained from Haida Pharmaceutical Co., Ltd. (Hangzhou, Zhejiang, China) and 4′,6-diamidino-2-phenylindole (DAPI) was purchased from the Beyotime Institute of Biotechnology (Haimen, Jiangsu, China). FAM-labelled scrambled siRNA (FAM-siRNA) was obtained from Biomics Biotechnologies Co., Ltd. (Nantong, Jiangsu, China) and the siRNA targeted to MDR-1 (sense: 5′-GUAUUGACAGCUAUUCGAAdTdT-3'; antisense: 3'-dTdTCAUAACUGUCGAUAAGCUU-5′) was bought from Shanghai GenePharma Co., Ltd. (Shanghai, China).

2.2. Cell culture

The human breast cancer cell line, Dox-resistant MCF-7 (MCF-7/ADR), was obtained from American Type Culture Collection (ATCC, Manassas, VA, USA). The cells were cultured in Dulbecco's Modified Eagle Medium (DMEM, Thermo Fisher Scientific, Waltham, MA, USA) supplemented with 10% fetal bovine serum (FBS, Thermo Fisher Scientific, Waltham, MA, USA) in a humidified incubator at 37 °C and 5% CO_2. The MCF-7/ADR cells were maintained in the presence of free Dox at 500 ng/mL in the culture medium.

2.3. Preparation and characterization of Nd-PC

The cationic supramolecular PC conjugates were synthesized as described previously [30]. The PC films were prepared by dropping 200 μL of 50 mg/mL of the PC solution onto a 1 cm × 1 cm silicon plate which was dried in air overnight. Afterwards, Nd ion implantation was conducted on a metal ion implanter (HEMII-80, Plasma Technology Ltd., Hong Kong SAR, China) equipped with a Nd cathodic arc source for 10 min at 20 kV to obtain Nd-PC. Four other metal elements including praseodymium (Pr), zirconium (Zr), molybdenum (Mo), and niobium (Nb) were also implanted into PC to obtain Pr-PC, Zr-PC, Mo-PC, and Nb-PC for comparison.

The elemental depth profiles and chemical states of the untreated PC, Nd-PC, as well as the other four metal-doped PC were determined by X-ray photoelectron spectroscopy (XPS, PHI 5802, Physical Electronics, Inc., Eden Prairie, MN, USA) with Al K_α irradiation. The sputtering rate was estimated to be approximately 7 nm/min based on a SiO_2 reference and the binding energies were referenced to the Au $4f_{7/2}$ line at 84.0 eV. The Nd, Pr, Zr, Mo, and Nb concentrations in the metal-doped PC were determined by inductively-coupled plasma optical emission spectroscopy (ICP-OES, PE Optima 2100DV, Perkin Elmer, Waltham, MA, USA). The coordinated contents of the incorporated elements were calculated from the total contents of the incorporated elements which were equal to those in the metal-doped PC dissolved in HNO_3 subtracted by those in the metal-doped PC dissolved in water. The Nd-PC was prepared by mixing the Nd-PC solution (50 mg/mL, 200 μL) with 50 μL of SiO_2 particles (D = 2.7 μm, 10% w/w, Microparticles GmbH, Berlin, Germany) electrostatically. Energy dispersive X-ray spectroscopy (EDS) was conducted on a transmission electron microscope (TEM, FEI Tecnai TF20, FEI Company, Hillsboro, OR, USA) at 200 kV.

2.4. Synthesis and characterization of PCD

The details about the synthesis of Ada-Dox and preparation of supramolecular PCD inclusion complexes were described in our previous paper [31]. In brief, Ada-COOH (35.2 mg, 0.19 mmol) and CDI (45.5 mg, 0.28 mmol, 1.5 equiv) were dissolved in DMSO (2 mL), added with triethylamine (200 μL), and stirred at room temperature under nitrogen. After 3 h, doxorubicin hydrochloride (93.3 mg, 0.17 mmol) dissolved in 1 mL of DMSO was slowly added to the Ada-CDI intermediate and the mixture was stirred overnight under nitrogen. After addition of distilled water to remove excess CDI, different amounts of PC (0.60 g, 1.80 g or 5.42 g) dissolved in H_2O (10–30 mL) were added dropwise to Ada-Dox. The resulting mixture was stirred for 8 h and the crude product was dialyzed against water for 1 day and freeze-dried. The purified PCD was obtained by removing excessive Ada-Dox by filtering the overnight-reacted mixture through silica gel.

^{1}H nuclear magnetic resonance (^{1}H NMR) spectra were acquired from Dox, Ada-COOH, Ada-Dox, PC, and PCD on the Varian Unity Inova 400 MHz spectrometer (Varian, Inc., Palo Alto, California, USA). 32 scans were acquired at room temperature after the drug and polymers were dissolved in 0.5 mL of DMSO-d_6 or deuterium oxide (D_2O). Two-dimensional nuclear overhauser effect spectroscopy (2D-NOESY) and nuclear magnetic resonance (NMR) were performed on the Bruker DRX-400 spectrometer (Bruker, Ettlingen, Germany) at room temperature using D_2O as the solvent. The UV–vis absorption spectra of Dox, PC, and PCD were acquired on a UV–vis spectrophotometer (Halo DB-20 UV/Visalbe Double Beam Spectrophotometer, Dynamica Scientific Ltd., Newport Pagnell, UK) and X-ray diffraction (XRD) was performed on a Rigaku D/max 2550PC diffractometer (Rigaku Corporation, Tokyo, Japan) with Cu K_α radiation.

2.5. Formation and characterization of the PCD/siRNA/Nd-PC nanoassemblies

The PCD/siRNA nanoassembly was prepared by mixing PCD with an equal volume of siRNA with a nitrogen/phosphorus (N/P) ratio of 15/1 and incubated at room temperature for 20 min. The PC or Nd-PC solution was added to the PCD/siRNA complexes and incubated for another 20 min at room temperature to produce the PCD/siRNA/PC or PCD/siRNA/Nd-PC nanoassembly. The final N/P ratio of the prepared nanoassembly was maintained at 30/1.

The particle size and zeta potential of the PCD/siRNA, PCD/siRNA/PC, and PCD/siRNA/Nd-PC complexes were determined by dynamic light scattering (DLS). Three measurements were performed on each sample using the Zetasizer Nano series Nano-ZS (Malvern Instruments Ltd., Malvern, UK) at 25 °C. The morphology of the complexes was examined by TEM (JEOL Ltd., Tokyo, Japan) and atomic force microscopy (AFM, Auto Probe CP, Park Scientific Instruments, Sunnyvale, CA, USA). Super-resolution stochastic optical reconstruction microscopy was performed on the DeltaVision Imaging OMX System (GE Healthcare, Little Chalfont, UK). In the investigation of the serum effects on the nanoassemblies, 100 μL of the aqueous PCD/siRNA/Nd-PC were mixed with 100 μL of FBS on 96-well plates at 37 °C. Aggregation of the PCD/siRNA/Nd-PC nanoassemblies was monitored in terms of turbidity by measuring the absorbance values at 630 nm on a microplate reader (BioTek Eon, BioTek Instruments Inc., Winooski,

Vermont, USA) [32].

2.6. In vitro drug release and cytotoxicity

The Dox loading content was determined on a UV–visible spectrophotometer (Halo DB-20 UV/Visalbe Double Beam Spectrophotometer, Dynamica Scientific Ltd., Newport Pagnell, UK). The PCD was dissolved in PBS and analyzed at $\lambda = 480$ nm. The calibration curve was established according to the absorption at the maximum emission wavelength of the PCD solution with different concentrations under the same conditions. The Dox loading content of PCD was calculated by the mass of the loaded Dox in the PCD over the mass of PCD X100%. The drug loading efficiency was calculated to be 5.5%. The drug release experiments were carried out in PBS at 37 °C at different pH of 5.0, 6.8, and 7.4 to simulate the normal blood and tumor surroundings. The PCD was dispersed in 1 mL of PBS and placed in a dialysis bag with a molecular weight cut-off of 8–14 kDa. The sealed dialysis bags were immersed in 50 mL of 1 × PBS and agitated at 100 rpm at 37 °C. At prescribed time intervals, 2 mL of the medium were taken out to measure the absorbance of Dox at 480 nm by UV–vis absorption and the same volume of fresh water was added. The amount of released Dox was calculated by comparing the calibration curves at each pH.

In the *in vitro* cytotoxicity evaluation, the MCF-7/ADR cells were seeded on 96-well plates at a density of 1×10^4 cells per well. After incubation for 24 h at 37 °C, the culture medium was discarded and the cells were treated with 200 μL fresh medium containing different concentrations of PC, Nd-PC, Dox, and PCD. After incubation for 48 h, 10 μL of MTT were added to each well and the plate was incubated for another 4 h. The solutions were then removed and the formazan crystals were dissolved in 100 μL DMSO. After gentle agitation for 15 min, the absorbance was monitored at 570 nm on a microplate reader (BioTek Eon, BioTek Instruments Inc., Winooski, Vermont, USA). The untreated cells served as the 100% cell viability control and the completely dead cells as the blank. The cytotoxicity was expressed as the percentage of the cell viability compared to the blank control. The relative cell growth (%) related to control cells was calculated by $([A]_{test}-[A]_{blank})/([A]_{control}-[A]_{blank}) \times 100\%$.

2.7. In vitro cellular uptake and cell apoptosis

Imaging of siRNA and Dox cellular uptake was conducted by confocal laser scanning microscopy (CLSM, Leica TCS SPE, Leica Microsystems, Wetzlar, Germany). In brief, the MCF-7/ADR cells (4×10^4 cells/well) were seeded on 24-well plates and incubated for 24 h. A series of serum-free medium containing FAM-siRNA, free Dox, PCD, PCD/FAM-siRNA, PCD/FAM-siRNA/PC, and PCD/FAM-siRNA/Nd-PC prepared described above were added and incubated with the cells for 4 h at 37 °C. The concentrations of equivalent free Dox and FAM-siRNA were 4 μg/mL and 200 nM, respectively. After removing the medium, the cells were washed twice with cold phosphate buffered saline (PBS) and fixed with 4% paraformaldehyde for 15 min. Finally, the cells were stained with DAPI for 10 min and washed with PBS twice prior to observation by CLSM. Fluorescence from the DAPI, Dox, and FAM-siRNA was triggered at 405 nm, 532 nm, and 488 nm and measured at emission ranges of 440–470 nm, 580–610 nm, and 500–530 nm, respectively.

In the cellular uptake studies by flow cytometry, the MCF-7/ADR cells were seeded on a 12-well plate at a density of 1.5×10^5 cells per well. After culturing for 24 h, the cells were incubated with FAM-siRNA, free Dox, PCD, PCD/FAM-siRNA, FAM-siRNA/PC, FAM-siRNA/Nd-PC, PCD/FAM-siRNA/PC, and PCD/FAM-siRNA/Nd-PC for 4 h at 37 °C. The concentrations of equivalent free Dox and FAM-siRNA were 2 μg/mL and 100 nM, respectively. The medium was aspirated and the cells were washed twice with cold PBS. The cells were then trypsinized, centrifuged, and washed twice by cold PBS. Finally, the samples were resuspended in 1 mL of PBS. 1×10^4 cells for each sample were analyzed for co-delivery of FAM-siRNA and Dox cellular uptake by flow cytometer (BD FACSCalibur, Becton, Dickinson and Company, Franklin Lakes, NJ, USA). The mean fluorescence intensity of the gated viable cells was quantified.

To examine the intracellular distribution of the complexes, the MCF-7/ADR cells were incubated with PCD/FAM-siRNA/Nd-PC or PCD/siRNA/Nd-PC complexes using a similar method for the cellular uptake observation by CLSM. After incubation for 12 h, the lysosomes were labeled with LysoTracker Deep Red ($E_x = 647$ nm, $E_m = 668$ nm) or LysoTracker Green DND-26 ($E_x = 504$ nm, $E_m = 511$ nm). The cells were then fixed with 4% paraformaldehyde and examined by CLSM.

Apoptosis of the MCF-7/ADR cells induced by the PCD/MDR-1/Nd-PC and other complexes was also investigated by flow cytometry. The MCF-7/ADR cells (8×10^4 cells/well) were seeded on 12-well plates and after incubation for 24 h, the cells were treated with the PCD, PCD/MDR-1, and PCD/MDR-1/Nd-PC complexes. The equivalent Dox and MDR-1 concentrations were 0.375 μg/mL and 100 nM, respectively. After incubation for 4 h, the medium was replaced by a fresh growth medium. After additional incubation for 48 h, the cells were rinsed twice with cold PBS, detached with the trypsin solution, and washed twice with cold PBS. They were diluted in 100 μL of the annexin-binding buffer at a density of approximately 1×10^6 cells/mL. 5 μL of annexin V FITC Conjugate and 10 μL of propidium iodide (PI) solution (Annexin V-FITC Apoptosis Detection Kit, Sigma-Aldrich, St. Louis, Missouri, USA) were added to 100 μL of the cell suspension and the cells were incubated in darkness for 10 min at room temperature. Afterwards, 400 μL of the annexin-binding buffer were added and mixed gently and the stained cells underwent flow cytometer to determine the fluorescence intensity.

The *in vitro* cytotoxicity of PCD/siRNA/Nd-PC, PC/siRNA, and PC/siRNA/Nd-PC was also investigated. The MCF-7/ADR cells were seeded on 96-well plates at a density of 1×10^4 cells per well. After incubation for 24 h at 37 °C, the culture medium was discarded and the cells were treated with 100 μL of serum-free medium containing PCD/siRNA/Nd-PC, PC/siRNA, and PC/siRNA/Nd-PC with different N/P ratios. After incubation for 5 h, the medium was replaced by a fresh growth medium. After further incubation for 48 h, the serum-free medium with 10 μL of MTT was added to each well and the plate was incubated for 4 h. The solutions were then removed and the formazan crystals were dissolved in 100 μL DMSO. After gentle agitation for 15 min, the absorbance was monitored at 570 nm on a microplate reader (BioTek Eon, BioTek Instruments Inc., Winooski, Vermont, USA). The cytotoxicity was calculated according to the method described above.

2.8. In vitro protein and mRNA regulation

The MCF-7/ADR cells were seeded on 6-well culture plates at a density of 5.0×10^5 cells per well and incubated at 37 °C in 5% CO_2 for 18 h to reach 70% confluence. The medium was replaced with 3 mL of fresh serum-free DMEM with free Dox, PCD, PCD/siRNA, PCD/siRNA/PC, PCD/siRNA/Nd-PC, PCD/siRNA/Pr-PC, PCD/siRNA/Zr-PC, PCD/siRNA/Mo-PC, and PCD/siRNA/Nb-PC containing 4 μg of siRNA. After incubation for 4 h, the medium was replaced by a fresh growth medium and the cells were further incubated for 48 h.

The cell proteins were extracted and cellular levels of CaM, metallothionein (MT), Caveolin1, Clathrin, P-gp, Bcl-2, Bax, and Caspase3 were assessed using the Western blot analysis. The total protein was quantified by the Pierce BCA protein assay kit (Thermo Fisher Scientific, Waltham, MA, USA). An equal amount of protein

was separated on the SDS-PAGE, transferred to the nitro-cellulose membrane, blocked, and incubated overnight with monoclonal antibodies against CaM, MT, Caveolin1, Clathrin, P-gp, Bcl-2, Bax, and Caspase3. After washing, the membrane was incubated with the HRP-conjugated secondary antibody for 2 h at room temperature. The bands were visualized using the Westzol enhanced chemiluminescence kit (iNtRON Biotechnology, Gyeonggi-do, Korea) and the expression was normalized to the house keeping gene (β-actin) expression.

Quantitative reverse transcription polymerase chain reaction (RT-PCR) was used in the analysis of the MCF-7/ADR cell lines expression of genes encoding CaM, MT, Caveolin1, Clathrin, P-gp, Bcl-2, Bax, and Caspase3 proteins. In the RT-PCR analysis, the cells were collected to extract mRNA and then reverse-transcribed into cDNA using the RNEasy Mini Kit (Qiagen, Hilden, Germany). The PCR parameters included 5 min of Taq activation at 95 °C, followed by 32 cycles of 95 °C × 30 s, 56 °C × 45 s, and 72 °C × 45 s. The relative gene expression values were calculated using the BandScan4.3 software and the data representing the CaM, MT, Caveolin1, Clathrin, P-gp, Bcl-2, Bax, and Caspase3 mRNA expressions were normalized to the housekeeping gene geneglyceraldehyde-3-phosphate dehydrogenase (GAPDH) as the endogenous reference. The eight genes and GAPDH in this study are listed in Table S1.

2.9. In vivo antitumor activity and immunohistology

Athymic female mice (BALB/c strain) (5–6 weeks old, 16–18 g) were acquired from the Zhejiang Chinese Medical University and maintained in a pathogen-free environment under controlled humidity and temperature. The animal experiments were performed in accordance with the China Animal Protection Law. The MCF-7/ADR cells were inoculated subcutaneously at an injection volume of 0.1 mL containing 1×10^7 cells at the abdominal of BALB/c nude mice, respectively.

The mice were assigned to six groups and treated with PBS, free Dox, PCD, PCD/MDR-1, PCD/MDR-1/PC, and PCD/MDR-1/Nd-PC at 0.5 mg/kg equivalent Dox and 6.5 μg of siRNA *via* intra-tumour injection when the tumour grew to a diameter of around 5 mm. Each treatment group consisted of eight mice (n = 8) for the antitumor therapy and three mice (n = 3) for RT-PCR and western blotting analysis. The treatment was performed twice a week for 3 weeks and tumor growth was monitored by calipers twice a week. The tumor volume (V) was calculated by the following formula: tumor volume V (mm^3) = $\pi/6 \times$ length (mm) × width $(mm)^2$. Three mice from each group were sacrificed 3 weeks later after the first injection. The tumors were dissected, weighed, and imaged. In the *in vivo* biodistribution study, PCD/FAM-siRNA/Nd-PC together with free Dox and FAM-siRNA as control groups was administrated to the tumor-bearing mice *via* intratumoral injection using similar method as described above. The Dox and FAM-siRNA fluorescence from the tumor-bearing mice was monitored by biofluorescence imaging after 1, 3, 6, and 12 h. The mice were sacrificed at 12 h after administration and the tumor, heart, liver, spleen, lung, and kidney were excised and imaged by the *in vivo* imaging system (FX Pro *In-Vivo* Imaging System, Kodak, Rochester, NY, USA). Magnetic resonance imaging (MRI) were conducted on the MesoMR60 (Shanghai Niumag Corporation, Shanghai, China) and the tumor vasculature conditions were also acquired by high-resolution photoacoustic imaging system (Vevo LAZR, FUJIFILM VisualSonics, Toronto, Canada) and multispectral optoacoustic tomography (MSOT) (iThera Medical GmbH, Munich, Germany). In the histological assay, the tumor tissues were fixed in 4% paraformaldehyde for 24 h. The specimens were dehydrated in graded ethanol, embedded in paraffin, and cut into 5-mm-thick sections. The fixed sections were deparaffinized and hydrated according to a standard protocol and stained with hematoxylin and eosin (H&E), CD31, Ki67, and MDR-1 immunohistochemistry before microscopic evaluation. The sections were examined on a Leica DM IL microscope (Leica Microsystems, Wetzlar, Germany). In the RT-PCR and western blotting analysis, the mice from each group were sacrificed 48 h after the last injection. The tumors were extracted and the rest of the process was the same as that described above.

2.10. Statistical analysis

The data are presented as means ± standard deviation (SD). Statistical analysis was performed using a standard Student's t -test with a minimum confidence level (P) of 0.05 for significant statistical difference.

3. Results

3.1. Characterization of PCD and Nd-PC

The supramolecular conjugate PCD is characterized by ^{1}H NMR (Fig. 2A and Fig. S1), UV–vis spectroscopy (Fig. 2B), 2D-NOESY NMR (Fig. S2), and XRD (Fig. S3). The characteristic peaks of PEI (δ 2.2–2.7 ppm, -$\underline{CH_2}CH_2NH$-) and HP-CD (δ 0.8–1.2 ppm, -$OCH_2CH(\underline{CH_3})OH$-) are observed and the weak peaks at δ 1.68 and 1.94 ppm in PCD are ascribed to the -CH- and -CH_2- groups in the adamantyl moiety (Fig. 2A, Fig. S1). In the UV spectrum, PC almost shows no UV absorption from 325 to 700 nm and Dox shows a broad absorption peak at around 480 nm. After Dox incorporation with PC, the absorption peak of Dox slightly shifts to 510 nm (Fig. 2B). The red-shifted peak in the UV–visible spectra is due to the host-guest interaction between the Dox molecules and polymers commonly observed from the Dox-polymer conjugates indicating complex formation and the phenomenon has also been observed by Chun et al. and Zhou et al. [33,34]. Supramolecular incorporation of Ada-Dox into HP-CD is confirmed by 2D-NOESY NMR. As shown in Fig. S2, the proton from the Ada moiety can be correlated with the inner protons of HP-CD core, indicating that Ada-Dox forms supramolecular inclusion complexes. This is further confirmed by XRD. Fig. S3 shows that the sharp peaks from Dox represent the channel-type crystal structure, whereas the broad peak of PC represents its amorphous structure. When PC forms supramolecular inclusion complexes with Dox by the host-guest interaction, the sharp peaks from Dox disappear providing strong evidence of the amorphous structure of PCD.

Incorporation of Nd as well as other four metals into PC is determined by XPS (Fig. 2C and Figs. S4–S9) and ICP-OES (Table S2). The XPS full spectrum reveals successful doping of Nd into PC and the high-resolution Nd 3d spectra of Nd-PC in Fig. 2C show two peaks at 982.6 and 1005.2 eV ascribed to the Nd-O bond. Compared to the untreated PC (Fig. S4), the O 1s peaks of Nd-PC shift to a lower binding energy of 530.8 eV attributed to its bond with Nd (Fig. S5). Doping with Pr, Mo, Zr, and Nb into PC is also confirmed by XPS (Figs. S6–S9). Fig. S5 demonstrates that the maximum Nd atomic concentration is 6.2% and it decreases with sputtering time, indicating that only a tiny amount of Nd is introduced into PC and Nd is mainly distributed in the near surface of PC. When Nd-PC is dissolved in an aqueous solution, the concentrations of coordinated Nd (in the form of Nd-O) and free Nd (Nd^{3+}) are 0.75 ‰ and 0.24 ‰, respectively (Table S2). The extremely small concentration of Nd incorporated into PC is expected to induce negligible systemic cytotoxicity. The EDS map acquired from the Nd-PC@SiO_2 particles discloses that Nd is evenly distributed on the SiO_2 particles suggesting a uniform Nd distribution on the PC polymers after dissolution and re-drying (Fig. 2D).

Fig. 2E shows that PCD is able to sustain Dox release under

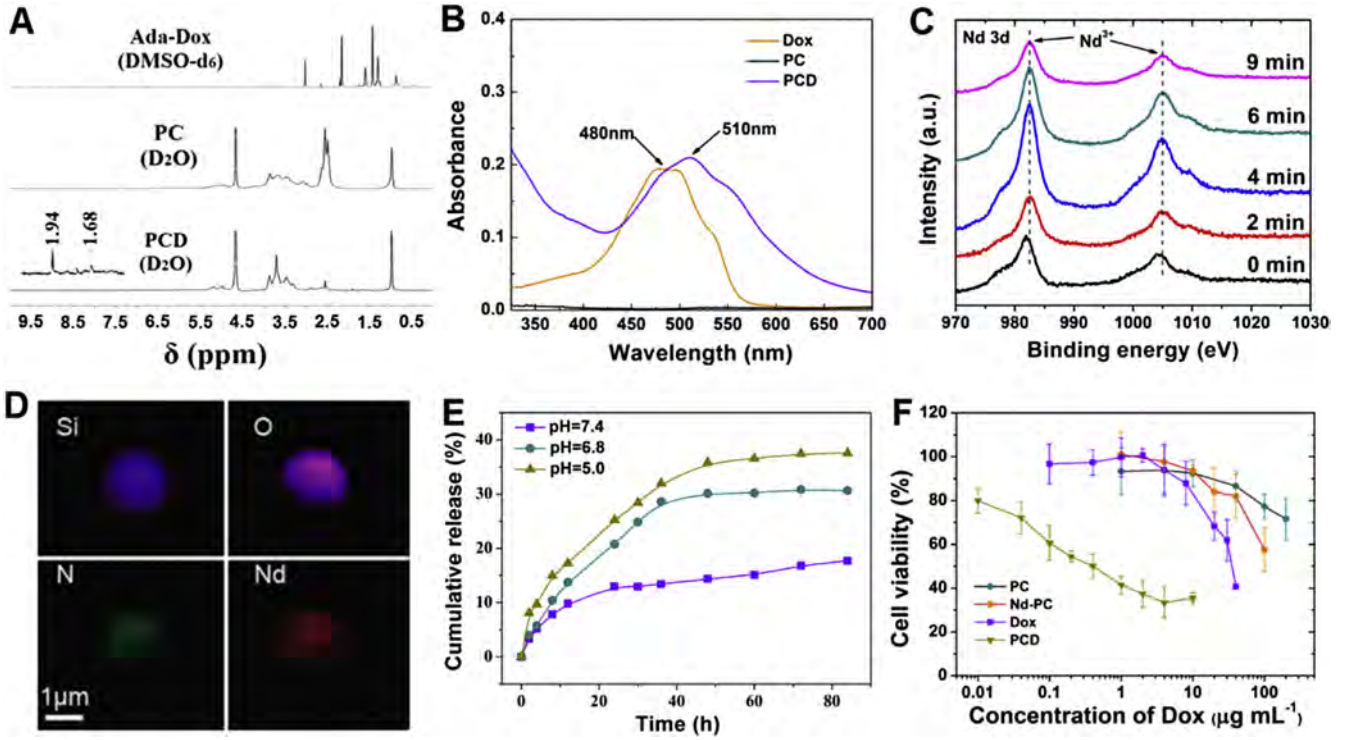

Fig. 2. Characterization of PCD and Nd-PC: (A) ^{1}H NMR spectra of Ada-Dox, PC, and PCD. (B) UV–vis spectra of Dox, PC, and PCD. (C) High-resolution XPS spectra of Nd 3d at different sputtering time. (D) EDS elemental maps of the Nd-PC@SiO2 microparticles. (E) *In vitro* Dox release from PCD in PBS at different pH values. (F) Viability of MCF-7/ADR cells after treated with PC, Nd-PC, Dox and PCD for 48 h. All the quantitative data represent mean ± SD (n = 3).

different pH conditions (pH = 7.4, 6.8, and 5.0) simulating the physiological condition, weak acidic condition in the tumor environment, and acidic endosome compartments, respectively. At a pH of 7.4, release of Dox from PCD is only 7.9% in the first 8 h and 17.7% within 84 h. Dox release increases dramatically with decreasing pH. At a pH of 5.0, the cumulative release of Dox increases to 15.0% in the first 8 h and as high as 37.6% within 84 h. The facilitated Dox release is attributed to dissociation of Ada-Dox from the CD cavity since the interaction between the acid solution and Ada becomes stronger than the weak hydrogen bond between Ada and CD under the acidic condition. This demonstrates that Dox release is facilitated at low pH and it may contribute to intracellular accumulation and life-time of Dox in the cancer cells. Therefore, Dox leakage can be retarded in the normal environment but effective release is allowed in the tumor and endosome environments. The *in vitro* cytotoxicity of Dox, PC, Nd-PC, and PCD against human breast drug-resistant cancer cell MCF-7/ADR is assessed by the MTT assay to investigate the 50% inhibitory concentration (IC_{50}) of the drugs and biocompatibility of the polymers. As shown in Fig. 2F, both PC and Nd-PC exhibit negligible toxicity in MCF-7/ADR cells at 40 μg/mL or lower concentrations, indicating that PC and Nd-PC have good biocompatibility in MCF-7/ADR cells. Compared to the free Dox, PCD exhibits significantly enhanced cytotoxicity in the MCF-7/ADR cells. The IC_{50} value of PCD is 0.4 μg/mL in MCF-7/ADR cells, which is smaller than that of the free Dox (34.0 μg/mL in MCF-7/ADR cells). The higher cell killing efficacy of PCD is attributed to efficient release of Dox from PCD into the cancer cells.

3.2. Characterization of the PCD/siRNA/Nd-PC nanoassemblies

The morphology and characteristics of the PCD/siRNA/Nd-PC nanoassembly are determined by DLS, TEM, AFM, and super-resolution microscopy (Fig. 3). The DLS results reveal that the PCD/siRNA/Nd-PC nanoassembly has a narrow size distribution between 225 and 243 nm with a N/P ratio between 20 and 45 (Fig. 3A). Fig. 3B shows that the PCD/siRNA/Nd-PC nanoassembly has a positive charge ranging from +16 to +18 mV with the N/P ratio from 20 to 45. No obvious changes in the particle size and zeta potential are observed from PC and Nd-PC, indicating that incorporation of Nd does not affect the nanoassembly characteristics. The particle size distribution determined by DLS and TEM confirm that the PCD/siRNA/Nd-PC tertiary nanoassembly has a larger diameter compared to the PCD/siRNA complex (Fig. 3C and D). After decoration of the PCD/siRNA complex with Nd-PC, the PCD/siRNA/Nd-PC nanoassembly is formed from the electrostatic interaction between the exposed negative siRNA and positive Nd-PC. The AFM images further confirm the spherical structure of the PCD/siRNA/Nd-PC nanoassembly with a diameter of approximately 200 nm and N/P ratio of 30 in good agreement with the DLS and TEM results (Fig. 3E). Super-resolution microscopy (Fig. 3F) indicates that Dox with the inherent red fluorescence signal is clearly visible within the green fluorescent shell of the FITC-labeled siRNA/Nd-PC complex, suggesting that Dox is located in the core of the PCD/siRNA/Nd-PC nanoassembly possibly as a result of strong hydrophobic interactions. As the PCD/siRNA/Nd-PC nanoassembly with an N/P ratio of 30 provides a suitable balance between the particle size and surface charge, this ratio is adopted in the subsequent study. As shown in Fig. S10, no significant increase in the turbidity is observed after incubation in 50% FBS for 24 h. It suggests no obvious aggregation, although the positively charged PCD/siRNA/Nd-PC complex may interact with negatively charged proteins in the serum.

3.3. Synergistic activities of siRNA and Dox in vitro

The cellular uptake of the Nd-integrated supramolecular

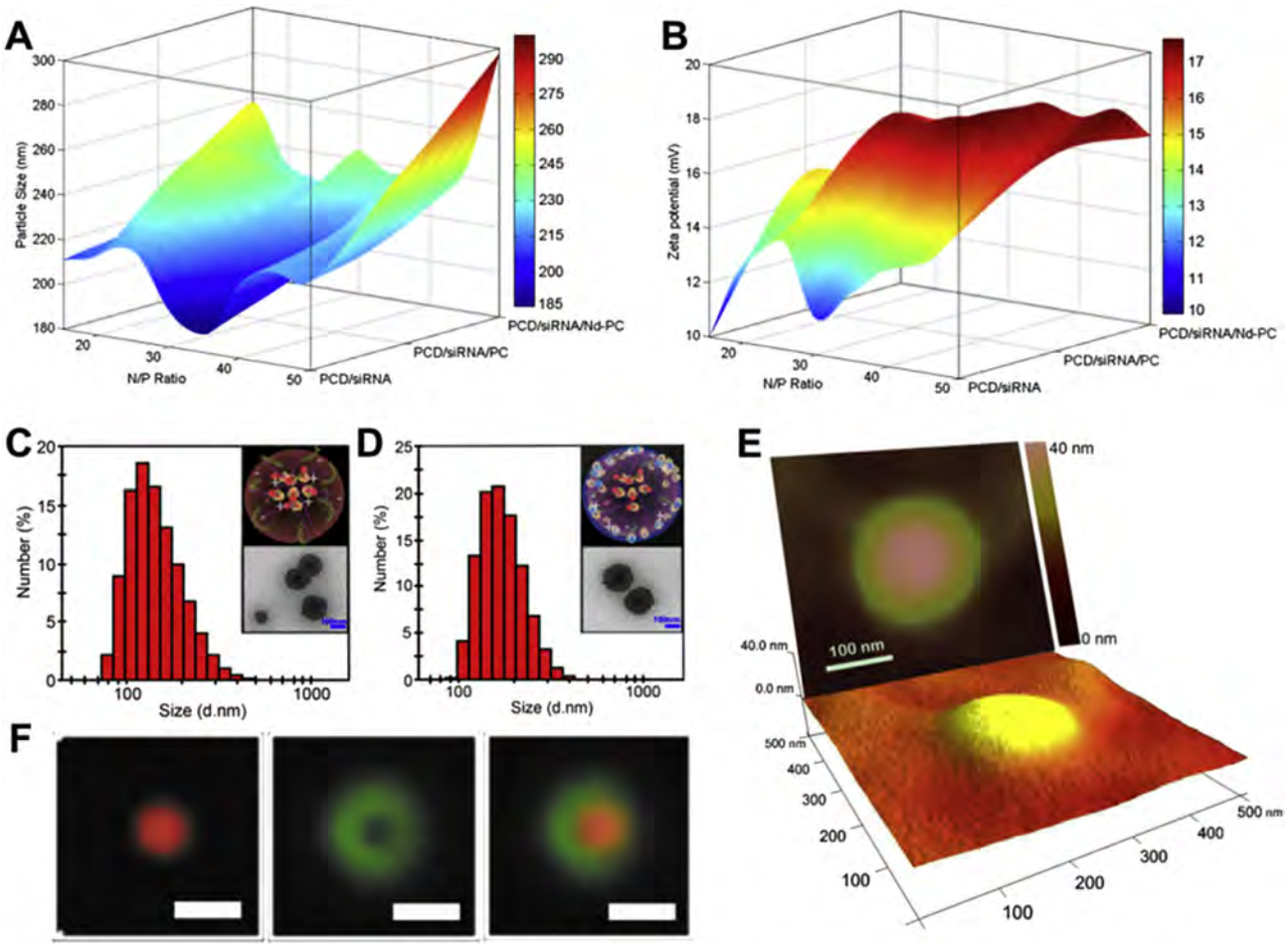

Fig. 3. Characterization of the PCD/siRNA, PCD/siRNA/PC, and PCD/siRNA/Nd-PC nanoassemblies: (A) Particle size and (B) zeta potential analysis of the PCD/siRNA, PCD/siRNA/PC, and PCD/siRNA/Nd-PC nanoassemblies with various N/P ratios by DLS. Particle size distribution, inserted schematic structure, and TEM images of (C) PCD/siRNA and (D) PCD/siRNA/Nd-PC with a N/P ratio of 30. (E) AFM amplitude image and height image of the PCD/siRNA/Nd-PC nanoassembly with a N/P ratio of 30. (F) Super-resolution microscopy images of the PCD/siRNA/Nd-PC nanoassembly with a N/P ratio of 30. The FAM-siRNA is shown in green and the drug Dox is shown in red. The scale bar is 200 nm. (For interpretation of the references to colour in this figure legend, the reader is referred to the web version of this article.)

nanoassembly and other formulations are evaluated with the MCF-7/ADR cells by CLSM (Fig. 4) and flow cytometry (Fig. 5A–D). The free Dox signal in the MCF-7/ADR is extremely weak while PCD exhibits strong red fluorescence. This is because the MCF-7/ADR cells can effectively pump the free Dox out. However, PCD can protect the loaded Dox and maintain fairly low initial release of Dox. Compared to the Nd-free formulations (FAM-siRNA, FAM-siRNA/PC and PCD/FAM-siRNA/PC), the Nd-integrated nanoassemblies (FAM-siRNA/Nd-PC and PCD/FAM-siRNA/Nd-PC) show higher levels of siRNA cellular uptake, suggesting that the outer layer, Nd-PC, is able to carry and deliver siRNA more efficiently (Figs. 4 and 5A and B). The PCD/FAM-siRNA nanoassembly without the outer layer PC or Nd-PC exhibits lower FAM-siRNA uptake level than PCD/FAM-siRNA/PC and PCD/FAM-siRNA/Nd-PC. This is because the siRNA exposed on the outer layer of the PCD/siRNA nanoassemblies tends to be prematurely released from the nanoassemblies and degraded by enzyme. The PCD/FAM-siRNA/Nd-PC-mediated uptake achieves a relatively high level of Dox but exhibits less Dox concentration in the MCF-7/ADR cells than that induced by PCD or PCD/FAM-siRNA after incubation for 4 h (Figs. 4 and 5C, and D). This indicates that the additional PC or Nd-PC layer with a positive charge may repel the charge-like Dox especially in the endosome/lysosome acid environment out of the nanoassemblies [35]. To observe the escape from lysosomes, the MCF-7/ADR cells treated with the PC/FAM-siRNA/Nd-PC or PCD/siRNA/Nd-PC complexes are stained with LysoTracker Red or LysoTracker Green, respectively. After incubation for 12 h, the intracellular FAM-siRNA is rarely colocalized with the lysosomes labeled with red fluorescent LysoTracker (Fig. S11A) and abundant red spots (Dox) are clearly separated from the green spots (Fig. S11B), indicating that the PCD/FAM-siRNA/Nd-PC complexes have a high efficiency to escape from the lysosome to the cytosol.

The viability of MCF-7/ADR cells after treatment with PCD/siRNA/Nd-PC, PC/siRNA, and PC/siRNA/Nd-PC with different formulations for 48 h are shown in Figs. S12 and S13. PC/siRNA exhibits negligible cytotoxicity to the MCF-7/ADR cells for a broad range of N/P ratios. The viability of the MCF-7/ADR cells incubated with PC/siRNA/Nd-PC decreases when N/P ratios increase to 40. At the N/P ratio of 30, the cell viability of the MCF-7/ADR cells mediated by the PC/siRNA/Nd-PC complexes reaches 97.1%, suggesting low toxicity and providing further proof that the optimal N/P ratio is 30 in the PCD/siRNA/Nd-PC system. The PCD/siRNA/Nd-PC assembly with the N/P ratio of 30 shows efficient killing of the MCF-7/ADR cells. The killing efficacy rises with increasing PCD concentration and stays at a high level even at low concentrations of the Nd-PC. Consequently, the killing ability of PCD/siRNA/Nd-PC is attributed to the combination of Dox, siRNA, and Nd-PC instead of the toxicity of Nd-PC. Analysis of cell apoptosis by flow cytometry

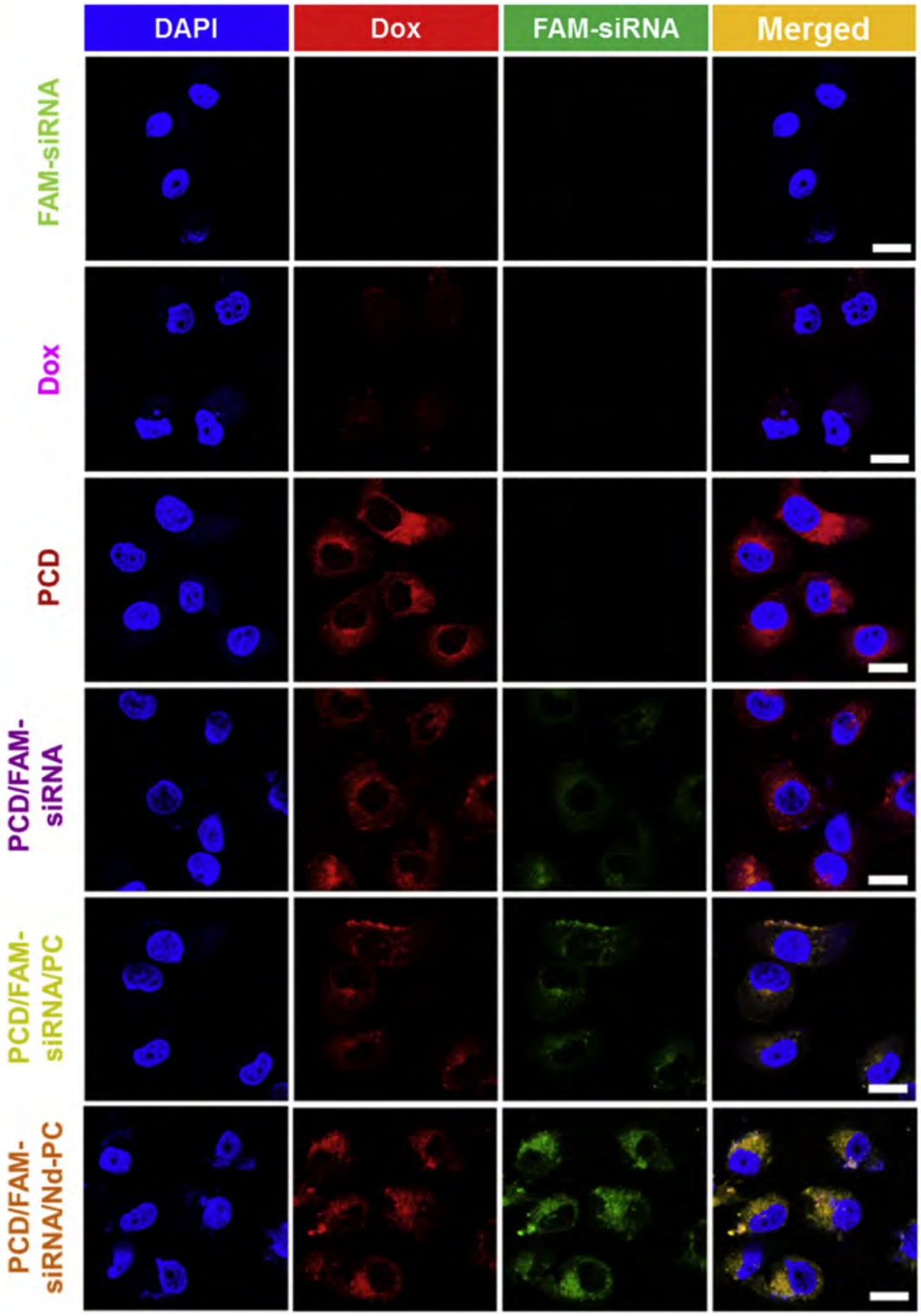

Fig. 4. *In vitro* cellular uptake of different formulations analyzed by CLSM. The CLSM images show uptake of FAM-siRNA and Dox in MCF-7/ADR cells after incubation for 4 h with different formulations. Cell nuclei were stained with DAPI. The bars represent 20 μm.

indicates that PCD/siRNA/Nd-PC induces the highest level of apoptosis in the MCF-7/ADR cells with a total apoptosis rate of 38.87% (Fig. 5E and Fig. S14). These results suggest that delivery of the PCD/FAM-siRNA/Nd-PC nanoassemblies induces multidrug-resistant cancer cells to apoptosis.

For further confirmation, the representative proteins related to cellular uptake, MDR, and cell apoptosis expressed in the MCF-7/ADR are analyzed by western blot analysis. As shown in Fig. 6A–C, both the CaM and MT are down-regulated by PC/siRNA/Nd-PC compared to other groups, but Caveolin1 and Clathrin are up-regulated after delivery of the PCD/siRNA/Nd-PC nanoassemblies. With regard to the apoptosis-related proteins, Bax and

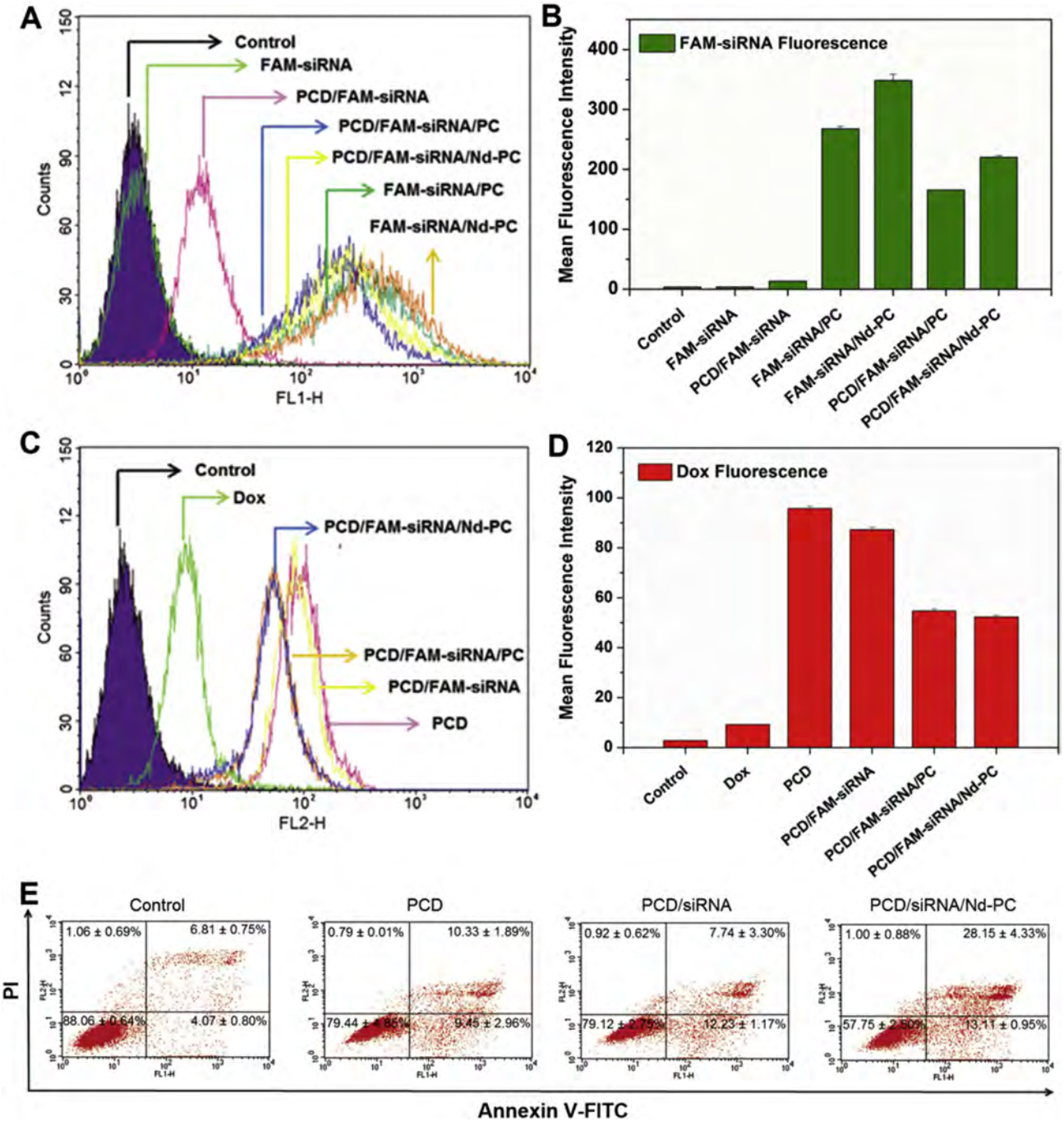

Fig. 5. *In vitro* cellular uptake of different formulations and induced cell apoptosis by flow cytometry. Qualitative and quantitative analysis of (A, B) FAM-siRNA and (C, D) Dox uptake in MCF-7/ADR cells after treatment with different formulations for 4 h by flow cytometry. (E) Analysis of MCF-7/ADR cell apoptosis induced by different formulations after 48 h treatment by flow cytometry. All the quantitative data represent mean ± SD (n = 3).

Caspase3 are significantly up-regulated, whereas the P-gp and Bcl-2 proteins are down-regulated. Regulation of the mRNA expression mediated by different formulations is assessed using the MCF-7/ADR cells with the GAPDH house-keeping gene as the normalization control. In general, the degree of mRNA expression correlates well with the protein expression. Regulation of the corresponding mRNA expression shows a similar trend as protein regulation (Fig. 6D). Up-regulation of Caveolin1, Clathrin, Bax, and Caspase3 is clearly observed from the MCF-7/ADR cell lines treated with the PCD/siRNA/Nd-PC nanoassembly, but the levels of CaM, MT, P-gp, and Bcl-2 mRNA expressions are down-regulated. Down-regulation of CaM, MT, P-gp, and Bcl-2 proteins and corresponding mRNAs induced by the PC/siRNA/Nd-PC nanoassemblies are the most significant compared to the nanoassemblies integrated with other metals (Pr, Zr, Mo, and Nb). Meanwhile, among all the groups, the PCD/siRNA/Nd-PC nanoassembly shows the highest upregulation of Caveolin1, Clathrin, Bax, and Caspase3 proteins and corresponding mRNAs (Fig. S15). These results suggest that the supramolecular nanoassembly integrated with Nd-PC shows the highest activity *in vitro*. Thus, Nd-PC is used as the decorating layer in the subsequent study.

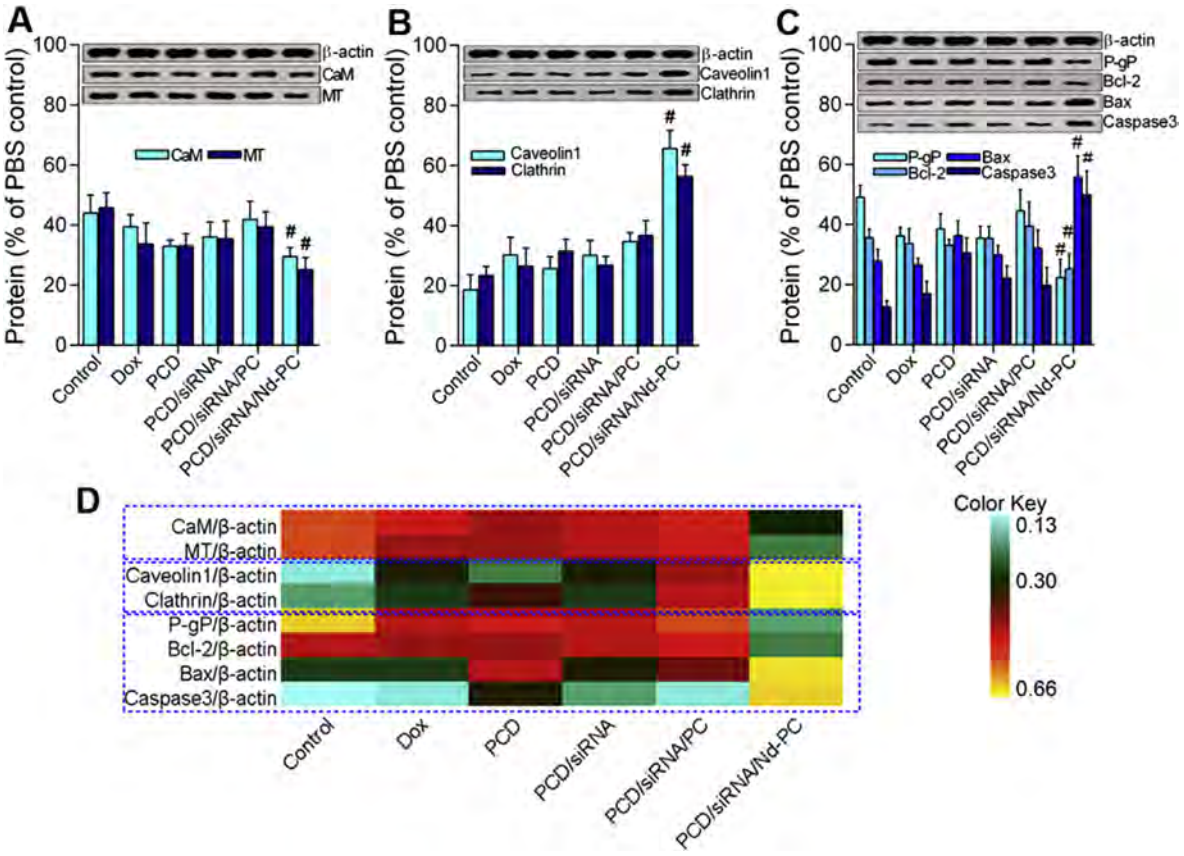

Fig. 6. *In vitro* regulation of proteins and mRNAs: *In vitro* (A, B, C) representative protein expression and analysis of light intensities analyzed by western blot. #P < 0.01, PCD/siRNA/Nd-PC vs PCD/siRNA/PC. The quantitative data represent mean ± SD (n = 3). (D) Heat map of the corresponding mRNA levels analyzed by RT-PCR. The higher color value represents the higher mRNA expression. (For interpretation of the references to colour in this figure legend, the reader is referred to the web version of this article.)

3.4. *In vivo* antitumor activity and immunohistology

Given the notable increase in cellular uptake and cell apoptosis as well as obvious regulation of proteins and mRNAs *in vitro*, the effects of the Nd-integrated supramolecular nanoassemblies on the antitumor activity are explored *in vivo*. As shown in Fig. 7A, the circled area denotes the tumor position. The tumor size decreases dramatically from the control to PCD/siRNA/Nd-PC groups and very weak MRI contrast is observed from the tumor position when the mice are administered with PCD/siRNA/Nd-PC. Fig. S16 and Fig. 7B shows that tumor growth is inhibited after intratumoral injection with either PCD/siRNA or PCD/siRNA/PC compared to the monotherapy groups (Dox and PCD). This indicates that delivery of siRNA and Dox produces synergistic effects against MDR tumor growth. The most effective therapy is achieved with PCD/siRNA/Nd-PC in tumor-bearing mice and the therapeutic effects are about 3 times more potent than those treated with either PCD/siRNA/PC or PCD/siRNA (Fig. 7C). Tumor weight analysis also validates that the PCD/siRNA/Nd-PC nanoassembly formulation as an effective nanotherapeutic agent against MDR tumor growth (Fig. 7D). The synergistic effects of the combination therapy are further enhanced by Nd integration into therapeutic nanoassembly. These results clearly demonstrate that tumor MDR can be effectively reversed by Nd integration into the supramolecular nanoassembly. *In vivo* fluorescence imaging is also used to monitor the time-dependent biodistribution of the PCD/FAM-siRNA/Nd-PC nanoassemblies. As shown in Fig. S17, the PCD/FAM-siRNA/Nd-PC nanoassemblies are mainly distributed in the tumor after intratumoral injection of PCD/FAM-siRNA/Nd-PC. The PCD/FAM-siRNA/Nd-PC nanoassemblies also show prolonged retention in the tumor compared to the free Dox and FAM-siRNA. Fig. S18 further confirms the strong signals from both Dox and FAM-siRNA in the PCD/FAM-siRNA/Nd-PC-treated tumors, but they are not detected from the liver and other organs.

The vascular density in the tumor tissues is determined by high-resolution ultrasound imaging (HRUI) and MSOT and the degree of blood oxygen saturation is analyzed by HRUI. The red pixels represent oxyhaemoglobin (HbO_2) and blue ones stand for deoxyhemoglobin (HbR). The high level of HbR and low level of HbO_2 corresponds to a small vascular density surrounding the tumor tissues. As shown in Fig. 8A, the tumor treated with PCD/siRNA/Nd-PC shows high HbR and low HbO_2 levels, suggesting reduced formation of vasculature. This is confirmed by the MSOT experiment in which a weak photoacoustic signal is detected from the tumor after treatment with the PCD/siRNA/Nd-PC nanoassembly (Fig. 8B and C). These results disclose that the most effective treatment against tumor growth is accomplished by delivering Dox and MDR-1 siRNA using the Nd-integrated supramolecular nanoassemblies.

Tumor cell apoptosis and proliferation in the tumors are analyzed by H&E staining as well as Ki67 and MDR-1 and CD31 assay after treatment with various formulations (Fig. 8D). The sections of tumor tissues from the PBS control and PCD group appear to be most hypercellular showing more obvious nuclear polymorphism. Among these therapeutic groups, the tumor tissues obtained after treatment with the PCD/siRNA/Nd-PC nanoassembly formulation show the fewest tumor cells and highest level of tumor necrosis. Immunohistochemical analysis of CD31 reveals a distinct decrease in the vessel density of the slice of MCF-7/ADR tumor

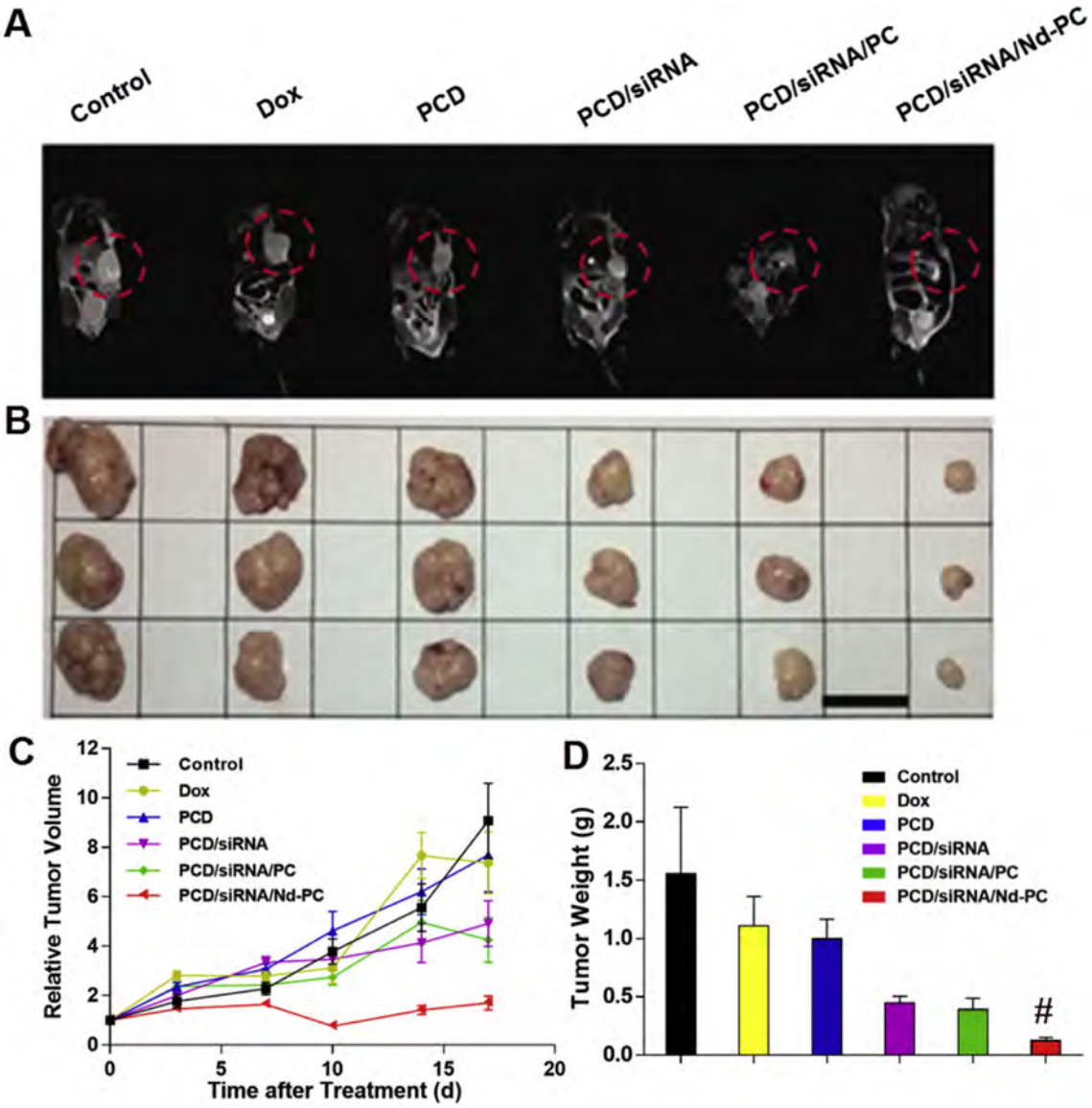

Fig. 7. *In vivo* antitumor activity. (A) MRI images of the tumor-bearing mice after treatment for 17 days. (B) Images of the tumors dissected from tumor-bearing mice treated with various formulations for 3, 10, and 17 days. Bar represents 2 cm. (C) Relative tumor volume in BALB/c nude mice with MCF-7/ADR xenografts with increasing time. (D) Weight of tumors dissected from mice after treatment for 17 days. #P < 0.01, PCD/siRNA/Nd-PC vs PCD/siRNA/PC. All the quantitative data represent mean ± SD (n = 3).

models after administration of PCD/siRNA/Nd-PC compared to PCD/siRNA, PCD/siRNA/PC, and other formulations. The Ki67 assay also shows that the Nd-integrated supramolecular nanoassembly reduces the percentage of proliferating Ki67-positive tumor cells, suggesting enhanced therapeutic efficacy in inhibiting tumor cell proliferation and apoptosis of tumor cells (Fig. S19). Analysis of the tumor tissues MDR-1 protein staining reveals a distinct decrease in the protein density of tumor slices after delivery of PCD/siRNA/Nd-PC nanoassembly compared to other formulations. These results supply additional evidence that the Nd-integrated supramolecular nanoassembly is effective in combating tumor MDR *in vivo*.

After *in vivo* treatment with the Nd-doped supramolecular nanoassembly, the proteins and corresponding mRNA expressions in the tumor tissues are analyzed by western blot and RT-PCR, respectively. In general, the *in vivo* protein regulations correlate well with the *in vitro* ones mediated by the Nd-integrated supramolecular nanoassembly and other formulations (Fig. 9A–C). Both CaM and MT are down-regulated but those of Caveolin1 and Clathrin are up-regulated after *in vivo* treatment with PCD/siRNA/Nd-PC. Similar to *in vitro* regulation, the apoptosis regulator, Bax and Caspase3, are also up-regulated and the P-gp and Bcl-2 proteins are down-regulated after the tumor-bearing mice are treated with PCD/siRNA/Nd-PC. In general, compared to other formulations such as PCD/siRNA or PCD/siRNA/PC, Nd integration further regulates proteins at the translational level, suggesting that the combination cancer therapy by siRNA and chemotherapeutics can be improved by surface functionalization with a rare earth element such as Nd. The mRNA expression at the transcriptional level also correlates with the protein regulation results (Fig. 9D).

4. Discussion

MDR to chemotherapy can be caused by different mechanisms including increased drug efflux and the failure to undergo drug-induced apoptosis presents a major challenge to cancer chemotherapy [36]. The most promising modality is to combine chemotherapy with the RNAi technique in a single treatment to achieve synergistic effects [37]. A functional vehicle delivering anticancer

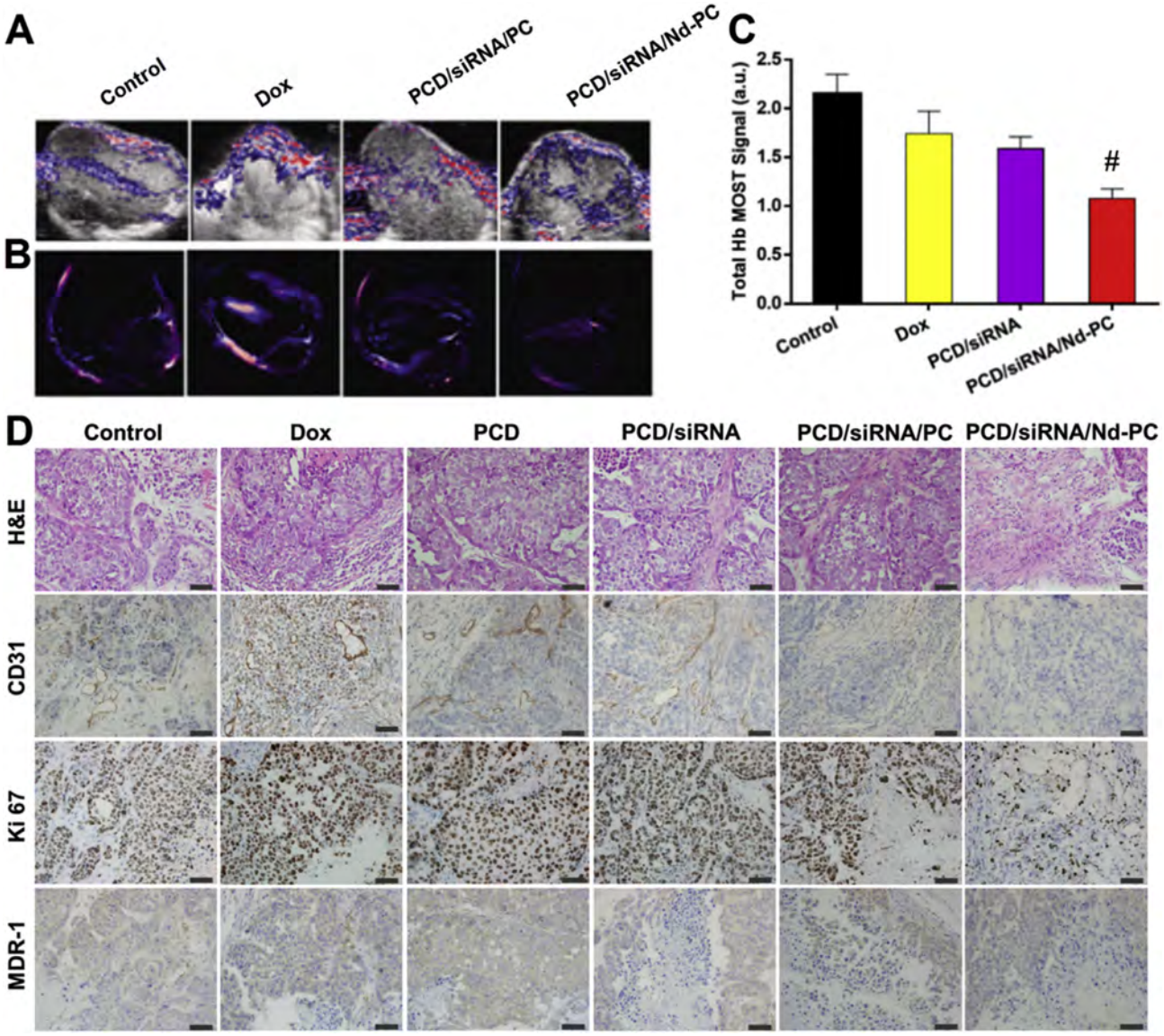

Fig. 8. *In vivo* antitumor activity. (A) Degree of blood oxygen saturation in the tumor tissues after treatment with PCD/siRNA/Nd-PC and other formulations evaluated by high-resolution ultrasound imaging system. (B) Photoacoustic images and (C) signal intensity of tumor vasculature after treatment with PCD/siRNA/Nd-PC and other formulations detected by multispectral optoacoustic tomography (MSOT). PBS is the control. #P < 0.01, PCD/siRNA/Nd-PC vs PCD/siRNA. The quantitative data represent mean ± SD (n = 3). (D) H&E, CD31, Ki67, MDR-1 analysis of the tumor tissue sections from the BALB/c nude mice with MCF-7/ADR xenografts after treatment for 17 days. The bars represent 50 μm.

drugs is crucial to anticancer therapies with high efficacy. In this work, we design and produce a multifunctional nanotherapeutic system PCD/siRNA/Nd-PC nanoassembly which integrates lanthanide elements with RNAi and chemotherapy to enhance the efficacy of cancer therapies both *in vitro* and *in vivo*. The PCD/siRNA/Nd-PC nanoassembly is formed by coating Nd-PC on the PCD/siRNA complexes which is firstly prepared through mixing PCD with siRNA.

Compared to the free Dox, PCD, PCD/siRNA, and PCD/siRNA/PC, the PCD/siRNA/Nd-PC nanoassembly exhibits effective tumor suppression due to three main reasons. Firstly, the PCD/siRNA/Nd-PC nanoassembly prepared with the cationic supramolecular polymeric nanoassembly has the proper particle size, moderate positive charge, and the cationic outer layer. The interaction between the nanoassembly and cell membrane is affected by the surface characteristics and to overcome the cell membrane obstacle is an essential step in cancer therapy. The proper particle size and moderate positive charge of PCD/siRNA/Nd-PC provide an important prerequisite for the cellular endocytosis. Meanwhile, the cationic polymers allows the nanoassembly to travel through the extracellular environment long enough to reach the tumor and facilitates the nanoassembly escape from the endosome *via* the 'proton-sponge' effect thereby avoiding premature degradation of the nanoassembly during delivery and ensuring efficient internalization and prolonged life-time of nanoassembly within the cancer cells. Therefore, the proper surface properties and cationic outer layer are important prerequisites for the PCD/siRNA/Nd-PC delivery system to achieve the desired therapeutic effects *in vivo*. The PCD/siRNA/Nd-PC nanoassembly shows enhanced penetration into the MCF-7/ADR cells through clathrin- and caveolin-mediated endocytosis. This is proven by up-regulation of Caveolin1 and Clathrin and corresponding mRNAs both *in vitro* and *in vivo*, since Caveolin1 is a major caveolae-coat protein involved in a variety of cell signaling processes and Clathrin is a protein that plays a major role in the formation of coated vesicles, vital parts to realize the clathrin-mediated endocytosis.

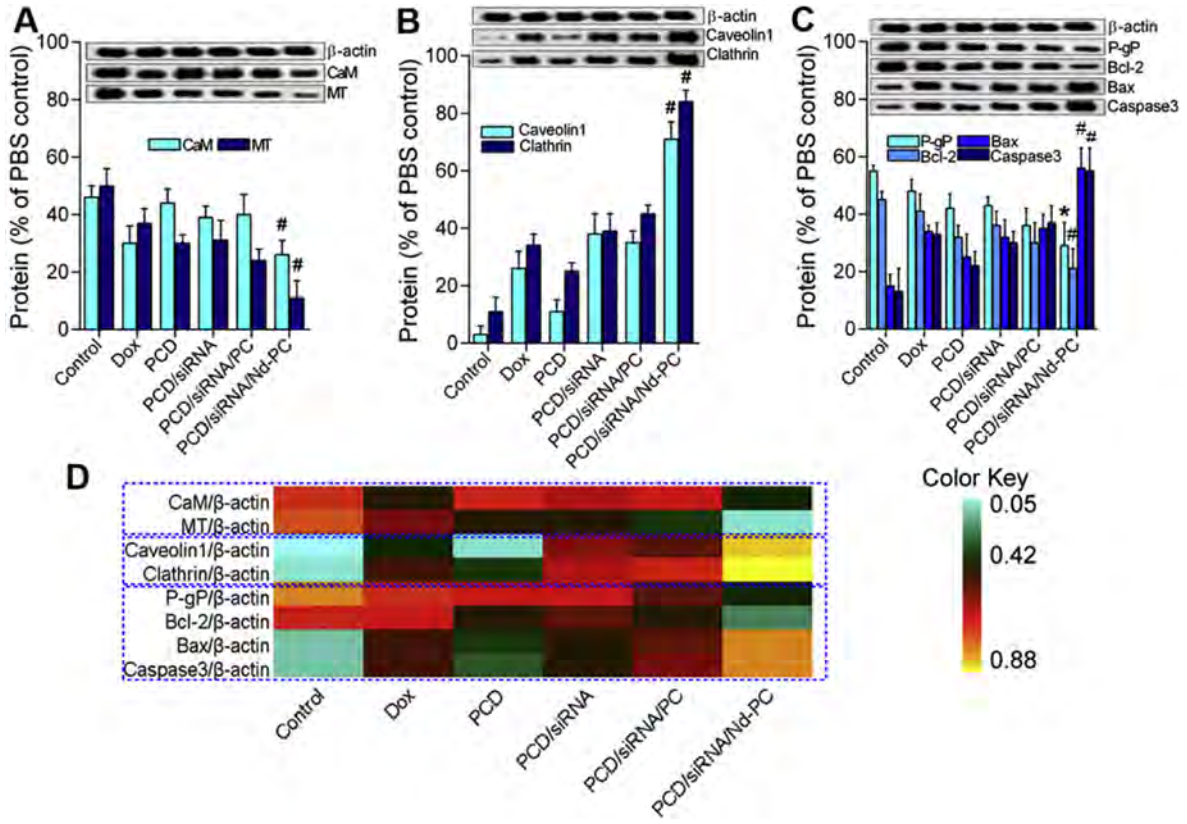

Fig. 9. *In vivo* regulation of proteins and mRNAs: *In vivo* (A, B, C) representative protein expression and analysis of light intensities analyzed by western blot. *P < 0.05 and #P < 0.01, PCD/siRNA/Nd-PC vs PCD/siRNA/PC. The quantitative data represent mean ± SD (n = 3). (D) Heat map of the corresponding mRNA levels analyzed by RT-PCR. The higher color value represents the higher mRNA expression. (For interpretation of the references to colour in this figure legend, the reader is referred to the web version of this article.)

Secondly, incorporation of a trace amount of Nd plays a vital role in the high performance of the PCD/siRNA/Nd-PC nanoassembly. Nd was reported to be tolerated by the various types of cells at relatively high concentrations [38] and our obtained results as well as our previous study [25] also revealed that the low cytotoxicity of the Nd-doped cationic polymers to various cell lines. Thus, the integrated Nd with a trace amount is expected to show good biocompatibility. The lanthanide element Nd in the outer layer of the PCD/siRNA/Nd-PC nanoassembly enhances the drug sensitivity to the MCF-7/ADR cells as indicated by down-regulation of CaM and up-regulation of MT. As an intracellular calcium-binding protein, CaM plays a vital role in many types of cellular activities in a calcium-dependent manner [39] and its antagonists such as trifluoperazine can increase the sensitivity of MDR cells to chemotherapy by inhibiting the voltage-dependent calcium channels and CaM [40–42]. Multidrug-resistant cancer cells are known to exhibit higher intracellular concentrations of Ca^{2+} than non-resistant ones [40]. Since lanthanide ions can be transported into cells through the calcium ion channel exchange pathway [16–18], it is reasonable to assume that Nd^{3+} released from the Nd-integrated nanoassembly may exchange calcium ions to decrease the intracellular concentration, as evidenced by down-regulation of CaM both *in vitro* and *in vivo*. On the other hand, MT is associated with resistance to toxicity due to the ability to interact with metal ions. It is regarded as the self-protection mechanism and they act as "sacrificial scavengers" to inactivate toxic molecules directly [43]. Down-regulation of MT mediated by the PCD/siRNA/Nd-PC nanoassembly *in vitro* and *in vivo* may provide evidence about the reduced resistance to toxic anticancer drugs. Hence, it is likely that Nd integration enhances the drug sensitivity to the MDR cancer cells through the down regulation of metal-binding proteins like MT.

Thirdly, efficient silencing of MDR-1 gene by the siRNA released from the PCD/siRNA/Nd-PC nanoassembly system combined with the Dox loaded in the inner layer contributes to the high killing efficacy of cancer cells. Release of siRNA is induced by the competitive interaction of the negatively charged substances in the cytoplasm such as heparin, which is a negatively charged polysaccharide and competes with the siRNA binding to cationic Nd-PC [28,29]. Ada-Dox may be detached from the cavity of CD in PCD followed by release of Dox under acidic and enzymatic conditions. The repulsive interaction between Nd-PC and residual PC with positive charges leads to dissociation of Nd-PC and PC in the cytoplasm. Over-expression of the drug efflux transporter P-gp, which is encoded by the MDR-1 gene, is a key factor of MDR in tumor cells [44]. P-gp belongs to the ATP-bind cassette (ABC) superfamily and transports a variety of structurally and functionally diverse chemotherapeutic drugs out of the intracellular compartments of MDR cells [45]. Hence, down-regulation of the P-gp expression mediated by the siRNA released from Nd-integrated supramolecular nanoassembly prevents Dox efflux. The released Dox is supposed to be efficiently transported to the nucleus to induce cancer cell apoptosis. The synergism between siRNA and Dox results in the greatly enhanced antitumor activity *in vivo*, which is proven by the down-regulation of Bcl-2 and reversed-regulation of Bax and Caspase3. The anti-apoptotic gene Bcl-2 which is known to overexpress in many types of cancer cells is related to tumorigenesis and chemoresistance [46,47]. Over-expression of Bcl-2 has been shown to delay the onset of apoptosis induced by several chemotherapeutic agents [48] and there is evidence that post-transcriptional silencing of Bcl-2 may be an effective approach to re-sensitize cancer cells to chemotherapeutic

drugs [49–52]. Notable downregulation of the Bcl-2 protein provides more evidence about the enhanced tumor cell response to chemotherapy *in vitro* and *in vivo* based on this study. Concurrently, activation of Caspase3, one of the most important enzymes in the pathways of therapeutic drug-induced apoptosis [53–55], attenuates the antiapoptotic activity in the drug resistant tumor cells both *in vitro* and *in vivo*. Furthermore, the Bax protein that is involved in p53-mediated apoptosis [56] is upregulated as typical hallmarks of apoptosis. All the evidence suggests that each building block from PCD/siRNA/Nd-PC may have specific functions thus providing multiple regulation mechanisms to combat cancer MDR at different delivery stages.

The protein network analysis in Fig. S20 shows the molecular networks and biological functions of the regulated proteins. It should be noted that the proteins investigated in this study are not independent and their functions are interrelated. For example, Caveolin1 is found to be associated with Bax, Caspase3, P-gp, and Bcl-2 in the protein network. Overexpression of Caveolin1 undermines the P-glycoprotein functions in Dox-resistant HS578T breast cancer cells by reducing the plasma membrane cholesterol level [57] and also inhibits mitogenic signaling to induce apoptosis [58,59]. Therefore, the regulated proteins by Nd-integrated supramolecular nanoassemblies may produce synergistic effects to reverse the tumor MDR. Collectively, synergistic tumor suppression can be realized by combining the distinctive functionality of the lanthanide element Nd, siRNA, and anticancer drug into an advanced therapeutic nanoassembly system. This piece of work discloses a novel and even universal approach to enhance tumor chemosensitivity by assembling Nd-integrated layers on polymeric nanoassemblies.

5. Conclusion

The Nd-integrated supramolecular polymeric nanoassembly constitutes a new type of multifunctional organic-inorganic nanotherapeutics for reversal of tumor MDR combining the advantages of the multifunctional properties of the lanthanide element to regulate MDR-restricted cellular uptake and drug efflux and offering the desirable features of cationic supramolecular polymers in the delivery of anticancer drugs and siRNA. The proper particle size and moderate positive charge provide the favorable conditions for premature degradation of siRNA in the physiological environment and promote efficient internalization of the PCD/siRNA/Nd-PC nanoassembly into cells. Surface integration of Nd enhances the drug sensitivity to the MCF-7/ADR cells and regulates P-gp function in combination with siRNA to prevent MDR-induced Dox efflux. These events are corroborated by the effective regulation of a number of proteins and related mRNA, including CaM, MT, caveolin1, clathrin, P-gp. In addition, the Nd-integrated supramolecular nanoassembly is capable of improving the overall therapeutic effects against tumor growth and enhances anti-angiogenesis and necrosis in the MDR murine tumor models *in vivo*. These results are supported by the regulation of the representative proteins and their related mRNAs, including Bcl-2, Bax, and Caspase3. The layered assembly of the Nd-integrated supramolecular nanoassembly not only is an effective tool to combat tumor MDR, but also provides a versatile strategy to improve the efficacy of polymeric nanomedicine by means of lanthanide integration to enhance the therapeutic effectiveness.

Acknowledgements

This work was jointly supported by Hong Kong Research Grants Council (RGC) General Research Funds (GRF) No. 11301215 as well as National Basic Research Program of China awarded to G. P. (973 Program, 2014CB931901). The authors also thank Mr. Hongzhen Bai for his assistance and suggestion on the schematic diagram.

Appendix A. Supplementary data

Supplementary data related to this article can be found at http://dx.doi.org/10.1016/j.biomaterials.2017.03.020.

References

[1] G. Szakacs, J.K. Paterson, J.A. Ludwig, C. Booth-Genthe, M.M. Gottesman, Targeting multidrug resistance in cancer, Nat. Rev. Drug Discov. 5 (2006) 219–234.
[2] N.S. Gandhi, R.K. Tekade, M.B. Chougule, Nanocarrier mediated delivery of siRNA/miRNA in combination with chemotherapeutic agents for cancer therapy: current progress and advances, J. Control. Release 194 (2014) 238–256.
[3] J. Wu, Y. Lu, A. Lee, X. Pan, X. Yang, X. Zhao, et al., Reversal of multidrug resistance by transferrin-conjugated liposomes co-encapsulating doxorubicin and verapamil, J. Pharm. Pharm. Sci. 10 (2007) 350–357.
[4] N.R. Patel, A. Rathi, D. Mongayt, V.P. Torchilin, Reversal of multidrug resistance by co-delivery of tariquidar (XR9576) and paclitaxel using long-circulating liposomes, Int. J. Pharm. 416 (2011) 296–299.
[5] M. Creixell, N.A. Peppas, Co-delivery of siRNA and therapeutic agents using nanocarriers to overcome cancer resistance, Nano Today 7 (2012) 367–379.
[6] A.K. Iyer, A. Singh, S. Ganta, M.M. Amiji, Role of integrated cancer nanomedicine in overcoming drug resistance, Adv. Drug Deliv. Rev. 65 (2013) 1784–1802.
[7] A.R. Kirtane, S.M. Kalscheuer, J. Panyam, Exploiting nanotechnology to overcome tumor drug resistance: challenges and opportunities, Adv. Drug Deliv. Rev. 65 (2013) 1731–1747.
[8] G.R. Whittell, M.D. Hager, U.S. Schubert, I. Manners, Functional soft materials from metallopolymers and metallosupramolecular polymers, Nat. Mater 10 (2011) 176–188.
[9] C. Sanchez, H. Arribart, M.M.G. Guille, Biomimetism and bioinspiration as tools for the design of innovative materials and systems, Nat. Mater 4 (2005) 277–288.
[10] E. Munch, M.E. Launey, D.H. Alsem, E. Saiz, A.P. Tomsia, R.O. Ritchie, Tough, bio-inspired hybrid materials, Science 322 (2008) 1516–1520.
[11] H. Jiang, S. Manolache, A.C.L. Wong, F.S. Denes, Plasma-enhanced deposition of silver nanoparticles onto polymer and metal surfaces for the generation of antimicrobial characteristics, J. Appl. Polym. Sci. 93 (2004) 1411–1422.
[12] M.W. Huh, I.K. Kang, D.H. Lee, W.S. Kim, D.H. Lee, L.S. Park, et al., Surface characterization and antibacterial activity of chitosan-grafted poly (ethylene terephthalate) prepared by plasma glow discharge, J. Appl. Polym. Sci. 81 (2001) 2769–2778.
[13] P.K. Chu, J. Chen, L. Wang, N. Huang, Plasma-surface modification of biomaterials, Mater. Sci. Eng. R. Rep. 36 (2002) 143–206.
[14] K.S. Smith, H.L. Huyck, An overview of the abundance, relative mobility, bioavailability, and human toxicity of metals, Environ. Geochem. Min. 6 (1999) 29–70.
[15] A. Kabata-Pendias, A.B. Mukherjee, Trace Elements from Soil to Human, Springer Science & Business Media, 2007.
[16] D.A. Powis, C.L. Clark, K.J. Obrien, Lanthanum can be transported by the sodium-calcium exchange pathway and directly triggers catecholamine release from bovine chromaffin cells, Cell Calcium 16 (1994) 377–390.
[17] J.P. Reeves, M. Condrescu, Lanthanum is transported by the sodium/calcium exchanger and regulates its activity, Am. J. Physiol. Cell Physiol. 285 (2003) C763–C770.
[18] Y.S. Gao, F.L. Zeng, A. Yi, S. Ping, L.H. Jing, Research of the entry of rare earth elements Eu3+ and La3+ into plant cell, Biol. Trace Elem. Res. 91 (2003) 253–265.
[19] L. Wang, J. Li, Q. Zhou, G. Yang, X.L. Ding, X. Li, et al., Rare earth elements activate endocytosis in plant cells, Proc. Natl. Acad. Sci. U. S. A. 111 (2014) 12936–12941.
[20] R.G. Canada, P.A. Andrews, K.M. Mack, A. Haider, The effects of terbium on the accumulation of cisplatin in human ovarian cancer cells, Biochim. Biophys. Acta, Mol. Cell Res. 1267 (1995) 25–30.
[21] K.M. Mack, P.A. Andrews, The effects of terbium on the cellular accumulation of cisplatin in MDA-MB-231 human breast tumor cells, Cancer Chemother. Pharmacol. 39 (1996) 217–222.
[22] Y.J. Ji, B. Xiao, Z.H. Wang, M.Z. Cui, Y.Y. Lu, The suppression effect of light rare earth elements on proliferation of two cancer cell lines, Biomed. Environ. Sci. 13 (2000) 287–292.
[23] T. Sato, M. Hashizume, Y. Hotta, Y. Okahata, Morphology and proliferation of B16 melanoma cells in the presence of lanthanide and Al3+ ions, Biometals 11 (1998) 107–112.
[24] S.-Y. Lee, I. Peckermann, E. Abinet, J. Okuda, G. Henze, A. Prokop, The rare-earth yttrium complex [YR (mtbmp)(thf)] triggers apoptosis via the extrinsic pathway and overcomes multiple drug resistance in leukemic cells, Med. Oncol. 29 (2012) 235–242.
[25] Q. Wang, W. Jin, G. Wu, Y. Zhao, X. Jin, X. Hu, et al., Rare-earth-incorporated

polymeric vector for enhanced gene delivery, Biomaterials 35 (2014) 479–488.
[26] Q. Hu, W. Li, X. Hu, Q. Hu, J. Shen, X. Jin, et al., Synergistic treatment of ovarian cancer by co-delivery of survivin shRNA and paclitaxel via supramolecular micellar assembly, Biomaterials 33 (2012) 6580–6591.
[27] Q.-D. Hu, H. Fan, Y. Ping, W.-Q. Liang, G.-P. Tang, J. Li, Cationic supramolecular nanoparticles for co-delivery of gene and anticancer drug, Chem. Commun. 47 (2011) 5572–5574.
[28] S. Sundaram, S. Viriyayuthakorn, C.M. Roth, Oligonucleotide structure influences the interactions between cationic polymers and oligonucleotides, Biomacromolecules 6 (2005) 2961–2968.
[29] A. Kwok, S.L. Hart, Comparative structural and functional studies of nanoparticle formulations for DNA and siRNA delivery, Nanomed. Nanotechnol. Biol. Med. 7 (2011) 210–219.
[30] G.P. Tang, H.Y. Guo, F. Alexis, X. Wang, S. Zeng, T.M. Lim, et al., Low molecular weight polyethylenimines linked by beta-cyclodextrin for gene transfer into the nervous system, J. Gene Med. 8 (2006) 736–744.
[31] Q. Jiang, P. Shi, C. Li, Q. Wang, F. Xu, W. Yang, et al., (Coixan polysaccharide)-graft-Polyethylenimine folate for tumor-targeted gene delivery, Macromol. Biosci. 11 (2011) 435–444.
[32] Q. Feng, M.-Z. Yu, J.-C. Wang, W.-J. Hou, L.-Y. Gao, X.-F. Ma, et al., Synergistic inhibition of breast cancer by co-delivery of VEGF siRNA and paclitaxel via vapreotide-modified core–shell nanoparticles, Biomaterials 35 (2014) 5028–5038.
[33] C. Chun, S.M. Lee, C.W. Kim, K.-Y. Hong, S.Y. Kim, H.K. Yang, et al., Doxorubicin-polyphosphazene conjugate hydrogels for locally controlled delivery of cancer therapeutics, Biomaterials 30 (2009) 4752–4762.
[34] T. Zhou, X.M. Zhou, D. Xing, Controlled release of doxorubicin from graphene oxide based charge-reversal nanocarrier, Biomaterials 35 (2014) 4185–4194.
[35] M. Dadsetan, Z. Liu, M. Pumberger, C.V. Giraldo, T. Ruesink, L. Lu, et al., A stimuli-responsive hydrogel for doxorubicin delivery, Biomaterials 31 (2010) 8051–8062.
[36] G. Szakács, J.K. Paterson, J.A. Ludwig, C. Booth-Genthe, M.M. Gottesman, Targeting multidrug resistance in cancer, Nat. Rev. Drug Discov. 5 (2006) 219–234.
[37] D. Castanotto, J.J. Rossi, The promises and pitfalls of RNA-interference-based therapeutics, Nature 457 (2009) 426–433.
[38] F. Feyerabend, J. Fischer, J. Holtz, F. Witte, R. Willumeit, H. Drücker, et al., Evaluation of short-term effects of rare earth and other elements used in magnesium alloys on primary cells and cell lines, Acta Biomater. 6 (2010) 1834–1842.
[39] Y. Mayur, S. Jagadeesh, K. Thimmaiah, Targeting calmodulin in reversing multi drug resistance in cancer cells, Mini Rev. Med. Chem. 6 (2006) 1383–1389.
[40] S. Nair, T.S.A. Samy, A. Krishan, Calcium, calmodulin, and protein content of adriamycin-resistant and -sensitive murine leukemic cells, Cancer Res. 46 (1986) 229–232.
[41] A. Fleckenstein, Specific pharmacology of calcium in myocardium, cardiac pacemakers, and vascular smooth muscle, Annu. Rev. Pharmacol. Toxicol. 17 (1977) 149–166.
[42] R.M. Levin, B. Weiss, Mechanism by which psychotropic drugs inhibit adenosine cyclic 3',5'-monophosphate phosphodiesterase of brain, Mol. Pharmacol. 12 (1976) 581–589.
[43] P.J. Thornalley, M. Vasak, Possible role for metallothionein in protection against radiation-induced oxidative stress. Kinetics and mechanism of its reaction with superoxide and hydroxyl radicals, Biochim. Biophys. Acta, Protein Struct. Mol. Enzymol. 827 (1985) 36–44.
[44] C.-H. Choi, ABC transporters as multidrug resistance mechanisms and the development of chemosensitizers for their reversal, Cancer Cell Int. 5 (2005) 1.
[45] G.D. Leonard, T. Fojo, S.E. Bates, The role of ABC transporters in clinical practice, Oncologist 8 (2003) 411–424.
[46] M.D. Berardo, R.M. Elledge, C.d. Moor, G.M. Clark, C.K. Osborne, D.C. Allred, bcl-2 and apoptosis in lymph node positive breast carcinoma, Cancer 82 (1998) 1296–1302.
[47] K. Tanabe, R. Kim, H. Inoue, M. Emi, Y. Uchida, T. Toge, Antisense Bcl-2 and HER-2 oligonucleotide treatment of breast cancer cells enhances their sensitivity to anticancer drugs, Int. J. Oncol. 22 (2003) 875–881.
[48] X.Y. Lei, M. Zhong, L.F. Feng, B.Y. Zhu, S.S. Tang, D.F. Liao, siRNA-mediated Bcl-2 and Bcl-xl gene silencing sensitizes human hepatoblastoma cells to chemotherapeutic drugs, Clin. Exp. Pharmacol. Physiol. 34 (2007) 450–456.
[49] M. Saad, O.B. Garbuzenko, T. Minko, Co-delivery of siRNA and an anticancer drug for treatment of multidrug-resistant cancer, Nanomedicine 3 (2008) 761–776.
[50] A. Pichler, N. Zelcer, J.L. Prior, A.J. Kuil, D. Piwnica-Worms, In vivo RNA interference–mediated ablation of MDR1 P-glycoprotein, Clin. Cancer Res. 11 (2005) 4487–4494.
[51] R.I. Pakunlu, T.J. Cook, T. Minko, Simultaneous modulation of multidrug resistance and antiapoptotic cellular defense by MDR1 and BCL-2 targeted antisense oligonucleotides enhances the anticancer efficacy of doxorubicin, Pharm. Res. 20 (2003) 351–359.
[52] R.I. Pakunlu, Y. Wang, W. Tsao, V. Pozharov, T.J. Cook, T. Minko, Enhancement of the efficacy of chemotherapy for lung cancer by simultaneous suppression of multidrug resistance and antiapoptotic cellular defense novel multicomponent delivery system, Cancer Res. 64 (2004) 6214–6224.
[53] J.C. Reed, Dysregulation of apoptosis in cancer, J. Clin. Oncol. 17 (1999), 2941-2941.
[54] L. Goyal, Cell death inhibition: keeping caspases in check, Cell 104 (2001) 805–808.
[55] M. Los, I. Herr, C. Friesen, S. Fulda, K. Schulze-Osthoff, K.-M. Debatin, Cross-resistance of CD95-and drug-induced apoptosis as a consequence of deficient activation of caspases (ICE/Ced-3 proteases), Blood 90 (1997) 3118–3129.
[56] X. Wu, Y. Deng, Bax and BH3-domain-only proteins in p53-mediated apoptosis, Front. Biosci. 7 (2002) 151–156.
[57] C. Cai, J. Chen, Overexpression of caveolin-1 induces alteration of multidrug resistance in Hs578T breast adenocarcinoma cells, Int. J. Cancer 111 (2004) 522–529.
[58] J.A. Engelman, R.J. Lee, A. Karnezis, D.J. Bearss, M. Webster, P. Siegel, et al., Reciprocal regulation of neu tyrosine kinase activity and Caveolin-1 protein expression in vitro and in vivo implications for human breast cancer, J. Biol. Chem. 273 (1998) 20448–20455.
[59] J.A. Engelman, C. Chu, A. Lin, H. Jo, T. Ikezu, T. Okamoto, et al., Caveolin-mediated regulation of signaling along the p42/44 MAP kinase cascade in vivo: a role for the caveolin-scaffolding domain, FEBS Lett. 428 (1998) 205–211.

Supporting Information

Lanthanide-Integrated Supramolecular Polymeric Nanoassembly with Multiple Regulation Characteristics for Multidrug-Resistant Cancer Therapy

Weihong Jin[a, 1], Qiwen Wang[b, c, 1], Min Wu[a, b], Yang Li[a, b], Guping Tang[a, b, *], Yuan Ping[d, *], Paul K. Chu[a, *]

[a] Department of Physics and Materials Science, City University of Hong Kong, Tat Chee Avenue, Kowloon, Hong Kong, China

[b] Institute of Chemical Biology and Pharmaceutical Chemistry, Zhejiang University, Hangzhou 310028, China

[c] Department of Cardiology, The First Affiliated Hospital, Zhejiang University School of Medicine, Hangzhou 310003, China

[d] School of Materials Science and Engineering, Nanyang Technological University, Singapore 639798, Singapore

[1]Both authors contributed equally to this work.

* To whom correspondence should be addressed:

Guping Tang – Tel.: +86-571-88273284; Fax: +86-571-88273284; E-mail: tangguping@zju.edu.cn.

Yuan Ping – E-mail: pingyuan7@gmail.com.

Paul K. Chu – Tel.: +852-34427724; Fax: +852-34420542; E-mail: paul.chu@cityu.edu.hk.

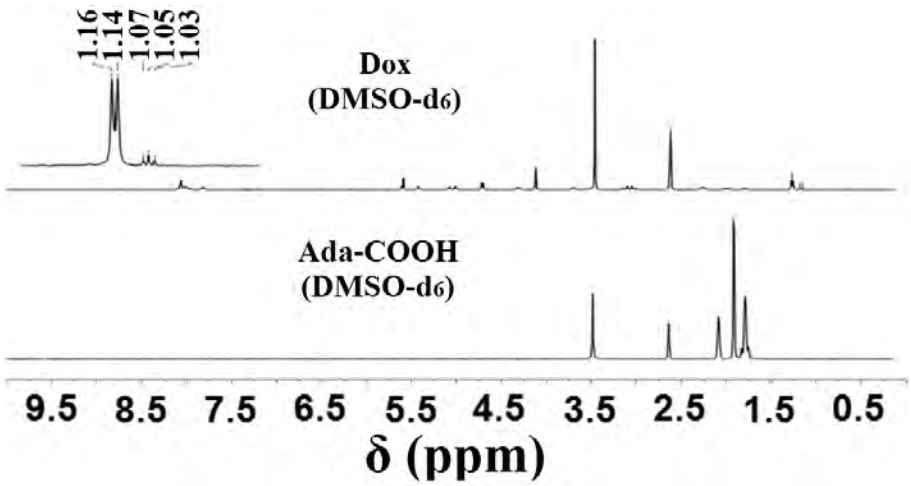

Fig. S1. ^{1}H NMR spectra of Dox and Ada-COOH.

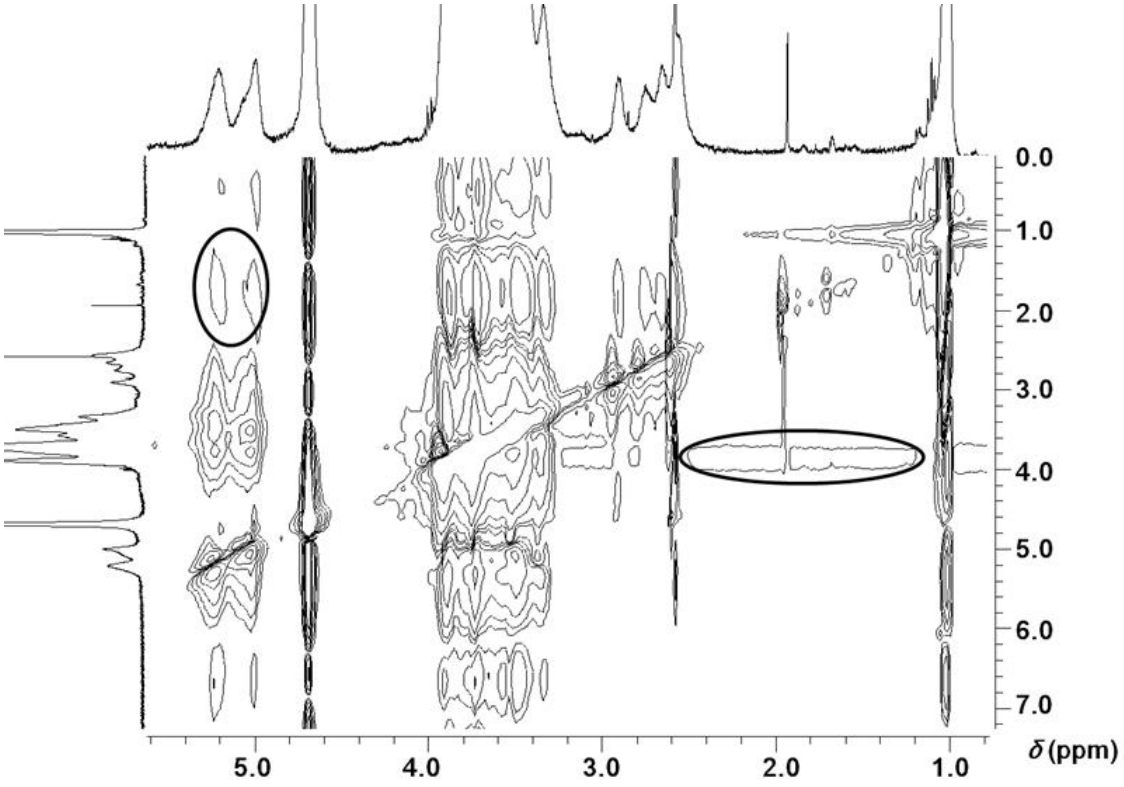

Fig. S2. 2D-NOESY NMR spectrum of PCD in D_2O.

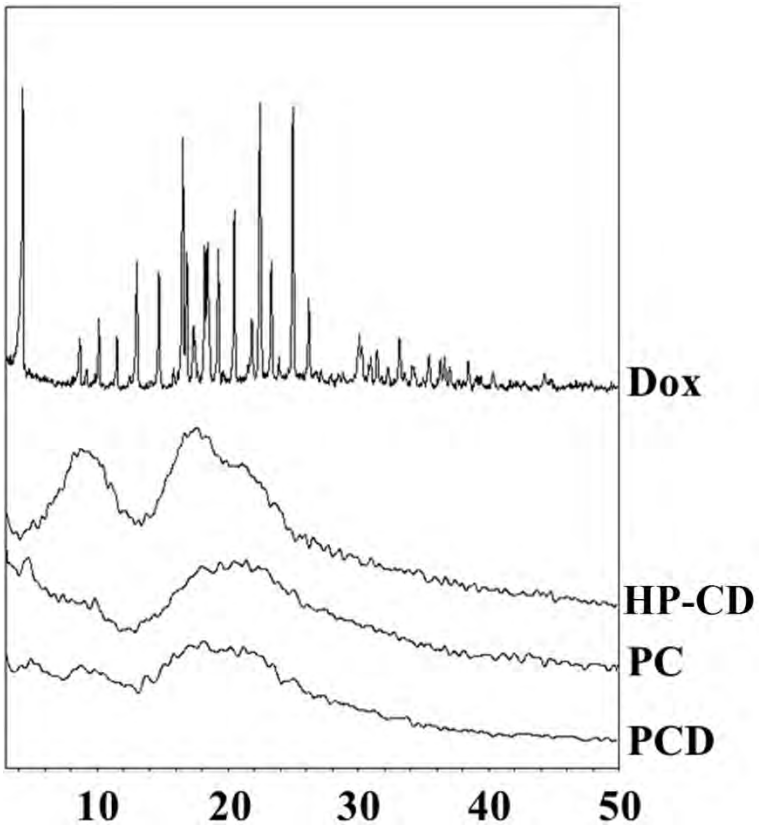

Fig. S3. X-ray diffraction spectra of Dox, hy-CD, PC, and PCD.

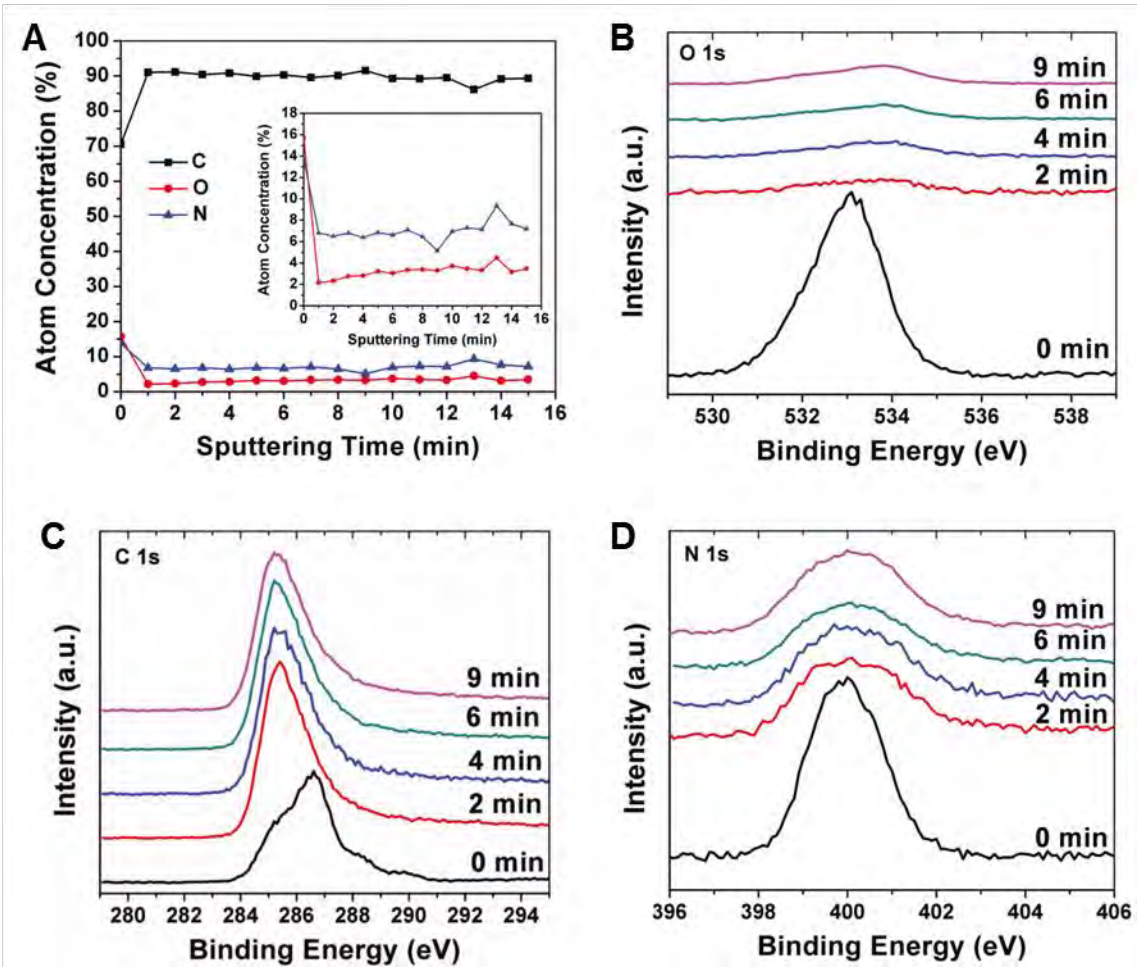

Fig.s S4. (A) XPS elemental depth profile of the untreated PC and high-resolution XPS spectra of (B) O 1s, (C) C 1s, and (D) N 1s after sputterin for different time.

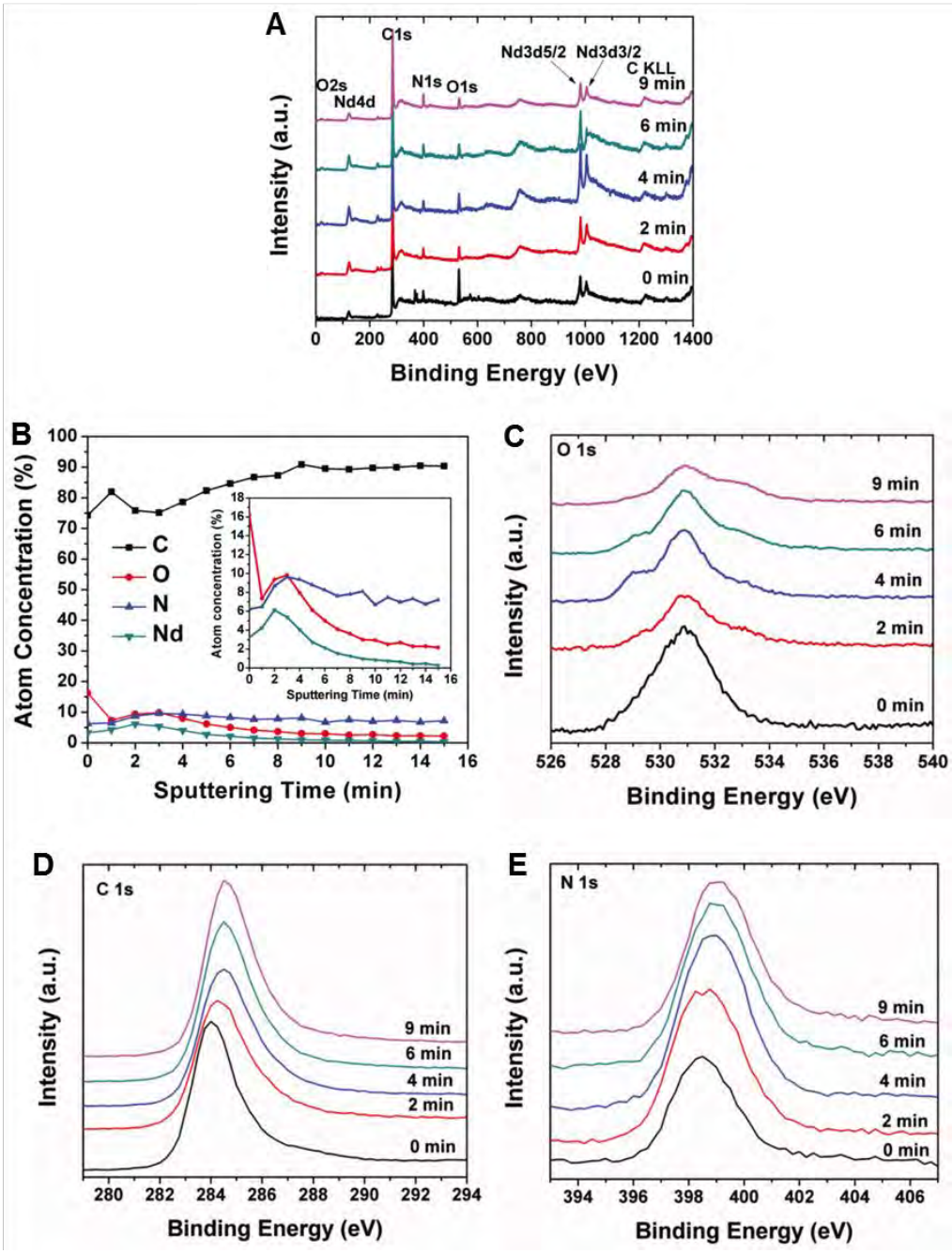

Fig. S5. XPS (A) full spectra and (B) elemental depth profile of Nd-PC and high-resolution XPS spectra of (C) O 1s, (D) C 1s, and (E) N 1s after sputtering for different time.

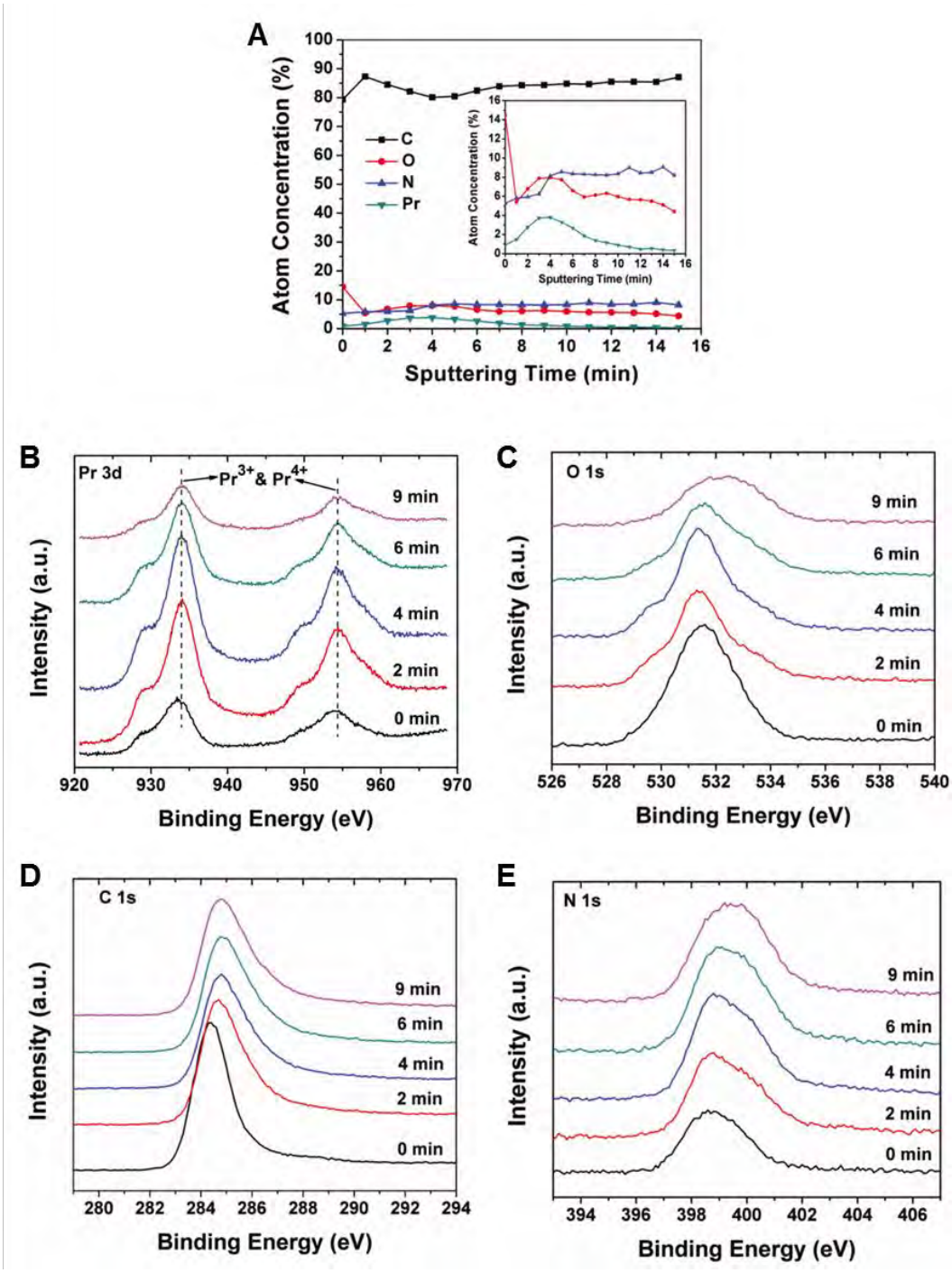

Fig. S6. (A) XPS elemental depth profile of Pr-PC and high-resolution XPS spectra of (B) Pr 3d, (C) O 1s, (D) C 1s, and (E) N 1s after sputtering for different time.

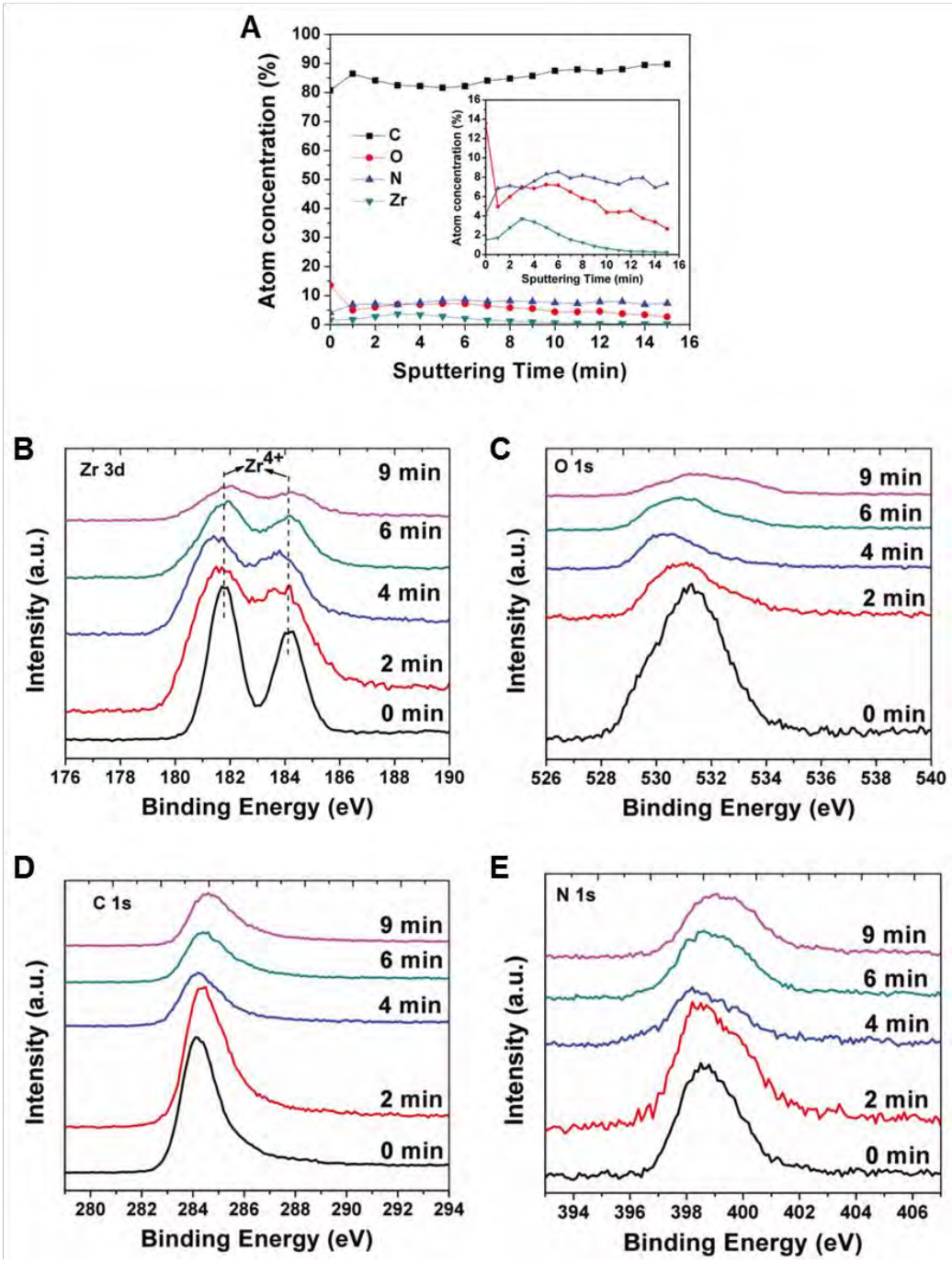

Fig. S7. (A) XPS elemental depth profile of Zr-PC and high-resolution XPS spectra of (B) Zr 3d, (C) O 1s, (D) C 1s, and (E) N 1s after sputtering for different time.

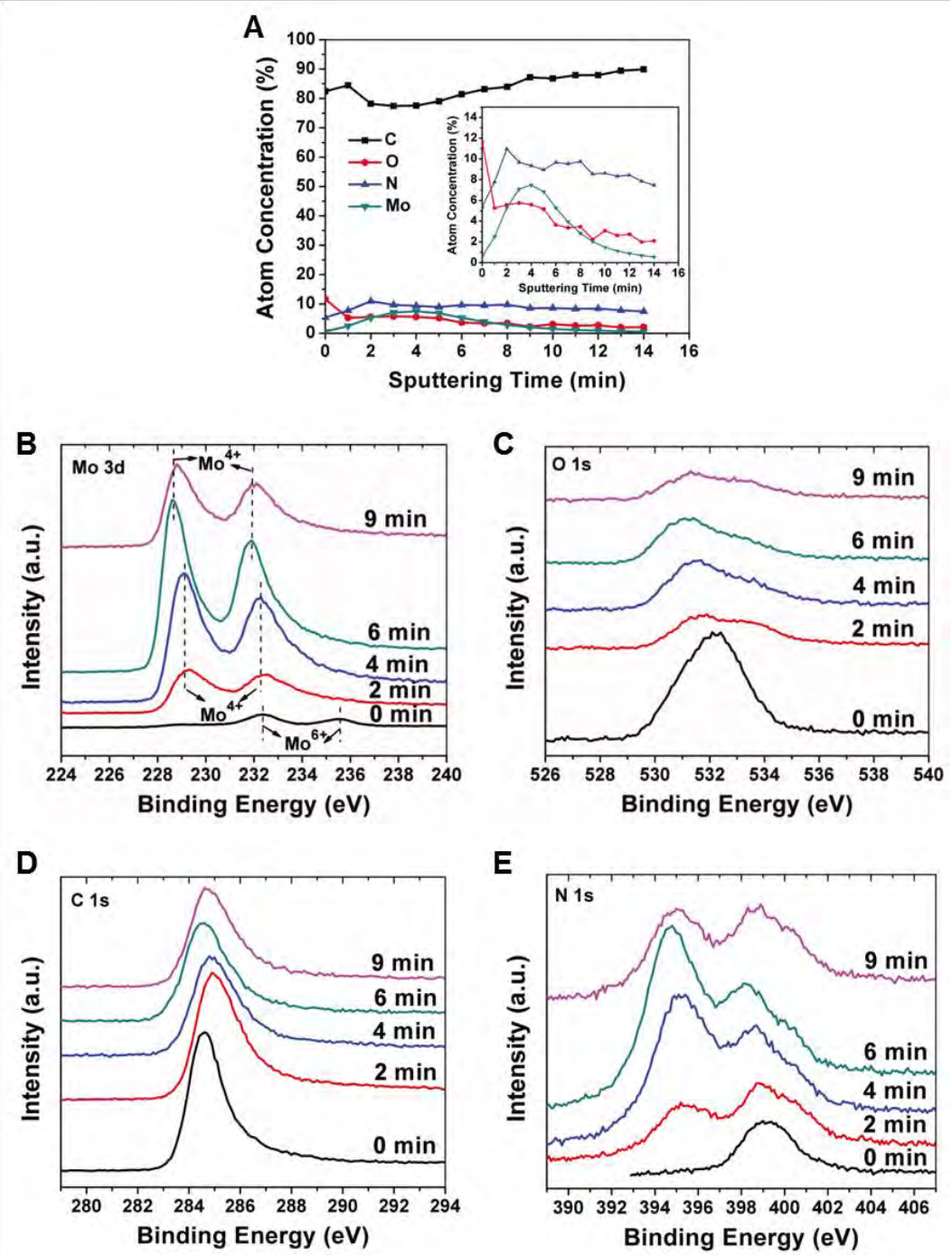

Fig. S8. (A) XPS elemental depth profile of Mo-PC and high-resolution XPS spectra of (B) Mo 3d, (C) O 1s, (D) C 1s, and (E) N 1s after sputtering for different time.

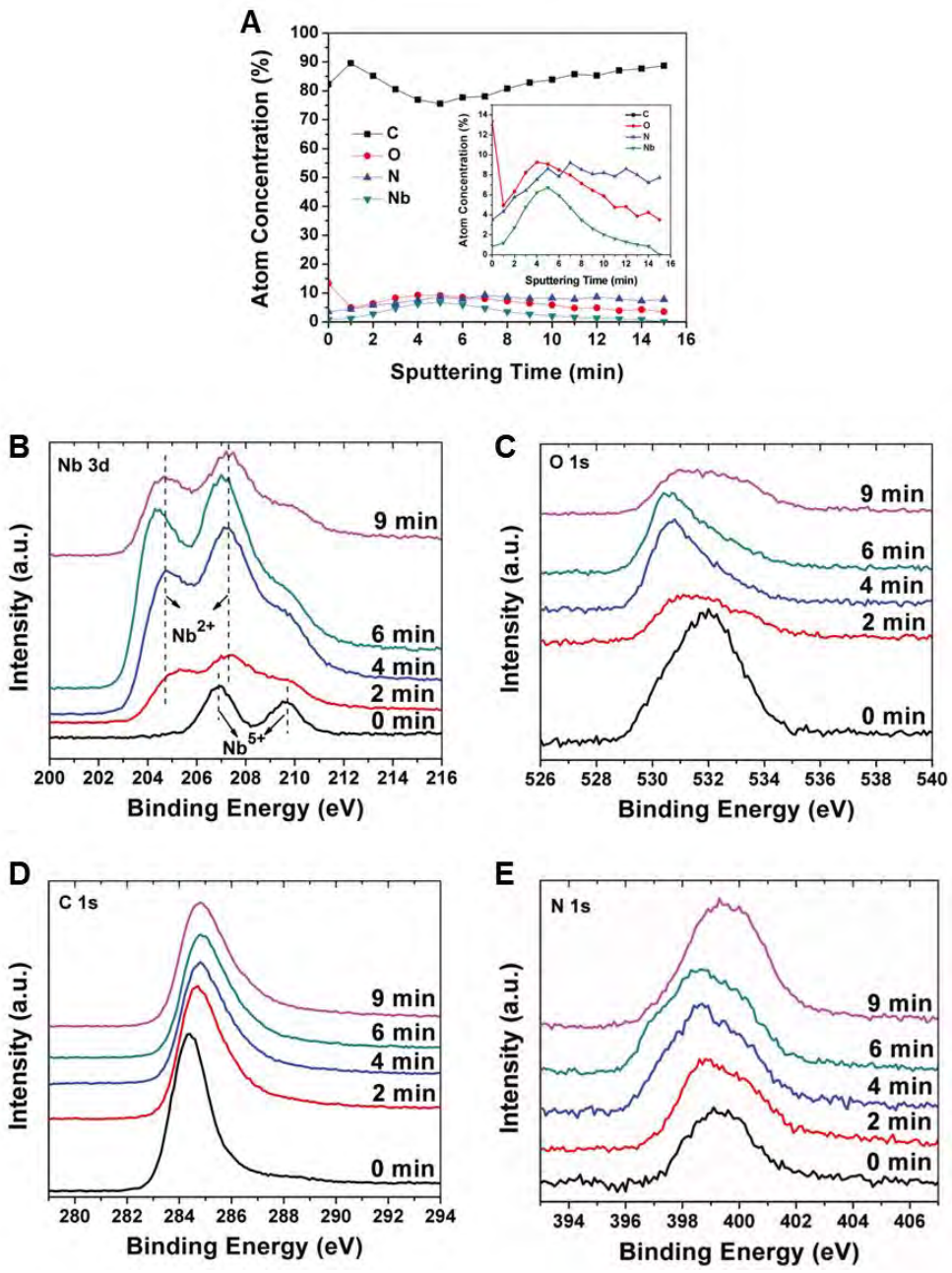

Fig. S9. (A) XPS elemental depth profile of Nb-PC and high-resolution XPS spectra of (B) Nb 3d, (C) O 1s, (D) C 1s, and (E) N 1s after sputtering for different time.

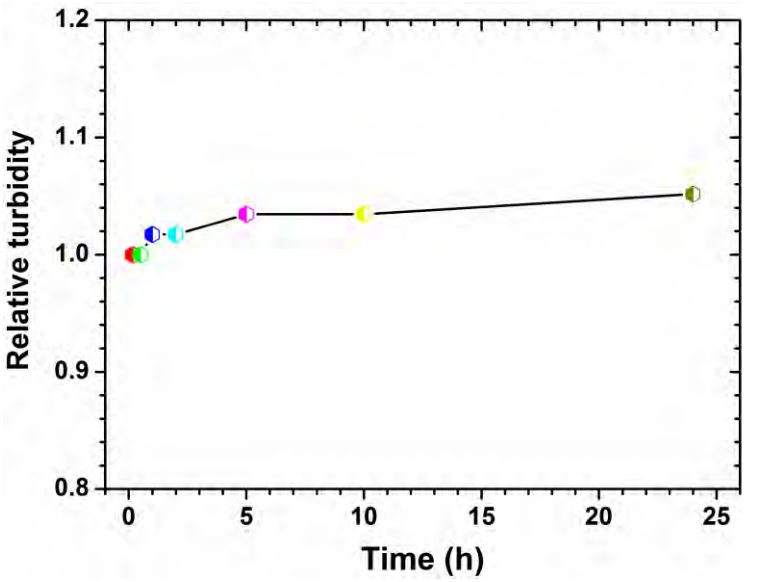

Fig. S10. Turdibity of the PCD/siRNA/Nd-PC nanoassembly in 50% FBS.

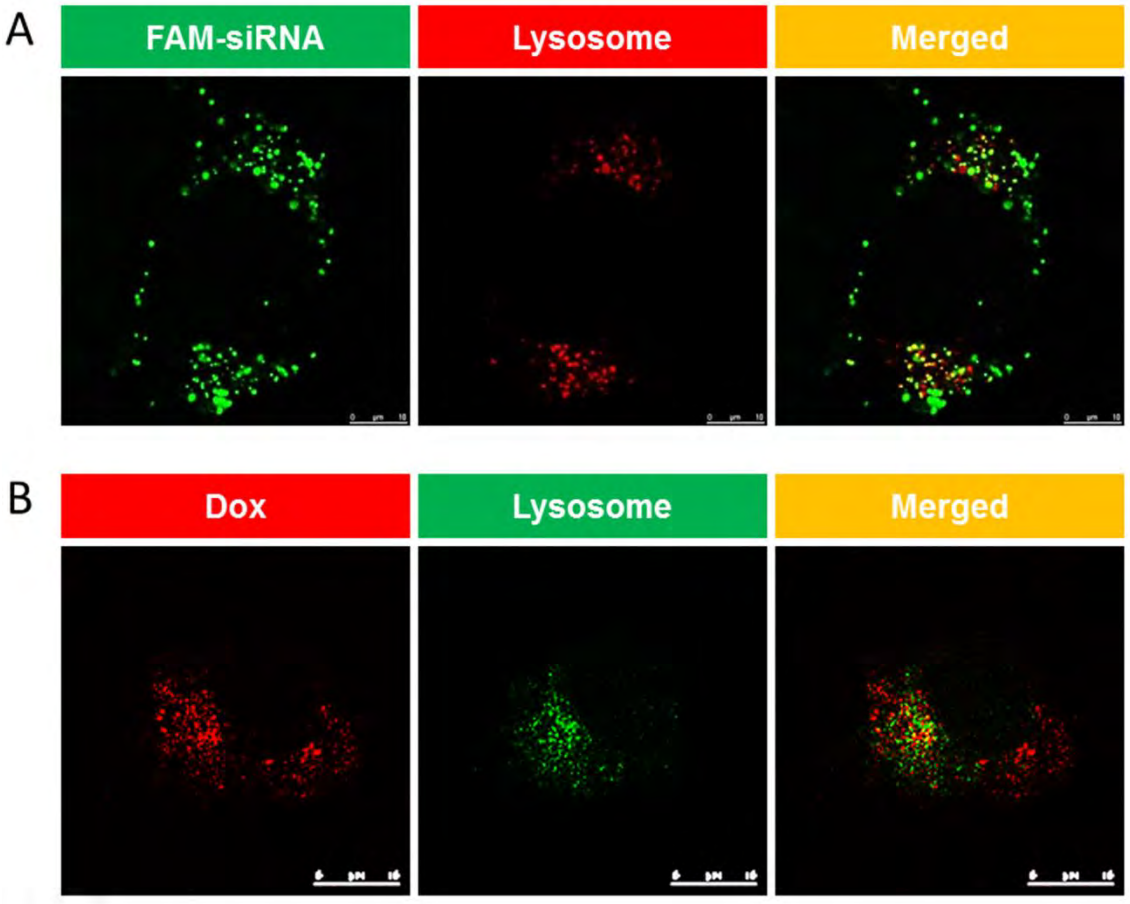

Fig. S11. Intracellular distribution of (A) PCD/FAM-siRNA/Nd-PC and (B) PCD/siRNA/Nd-PC in MCF-7/ADR after 12 h incubation. Cell nuclei were stained with DAPI. Endosomes/lysosomes were stained by Lyso Tracker Red for A and by Lyso Tracker Green for B, respectively. The bars represent 10 μm.

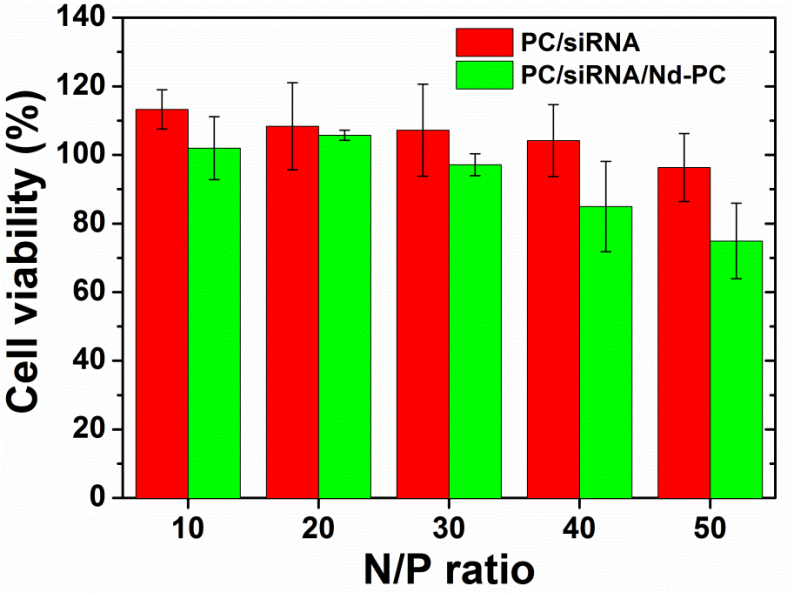

Fig. S12. Viability of MCF-7/ADR cells after treatment with PC/siRNA and PC/siRNA/Nd-PC with different N/P ratios for 48 h. All the quantitative data represent mean ± SD (n = 3).

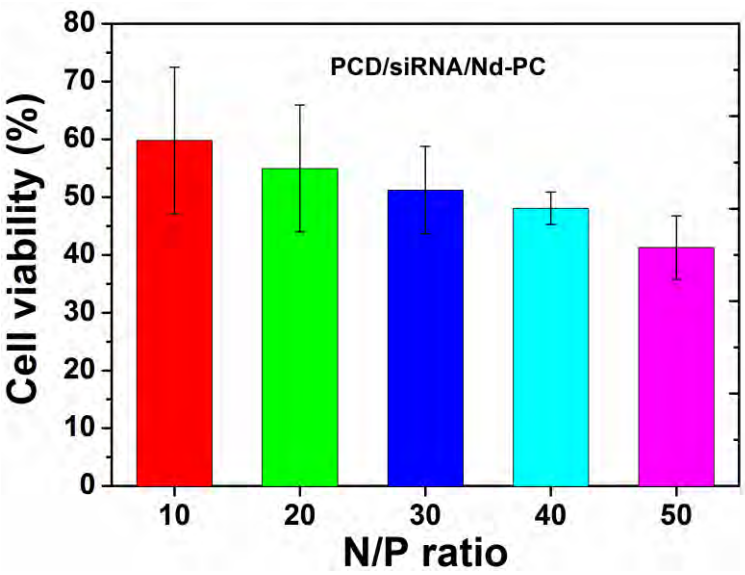

Fig. S13. Viability of MCF-7/ADR cells after treatment with PCD/siRNA/Nd-PC with different N/P ratios for 48 h. All the quantitative data represent mean ± SD (n = 3).

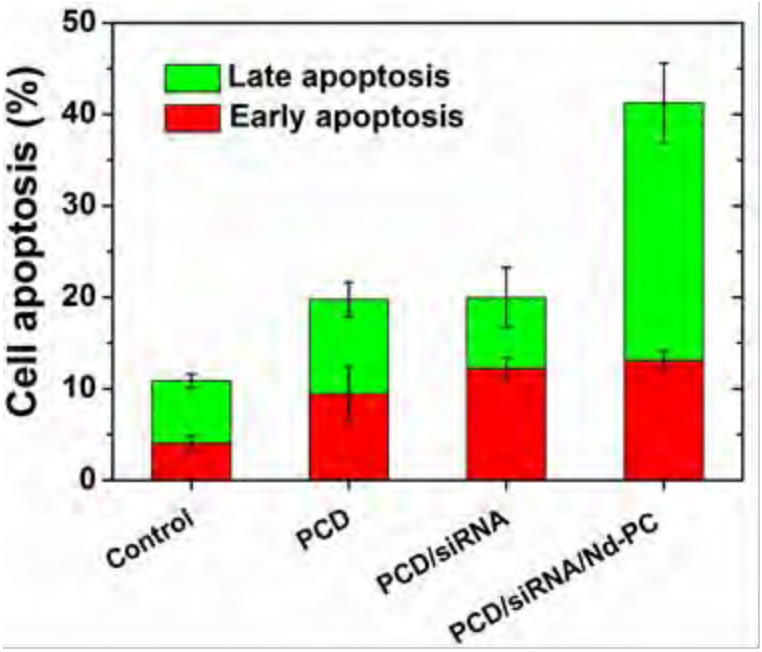

Fig. S14. Flow cytometry analysis of MCF-7/ADR cell apoptosis induced by PCD, PCD/siRNA, or PCD/siRNA/Nd-PC after treatment for 48 h. All the quantitative data represent mean ± SD (n = 3).

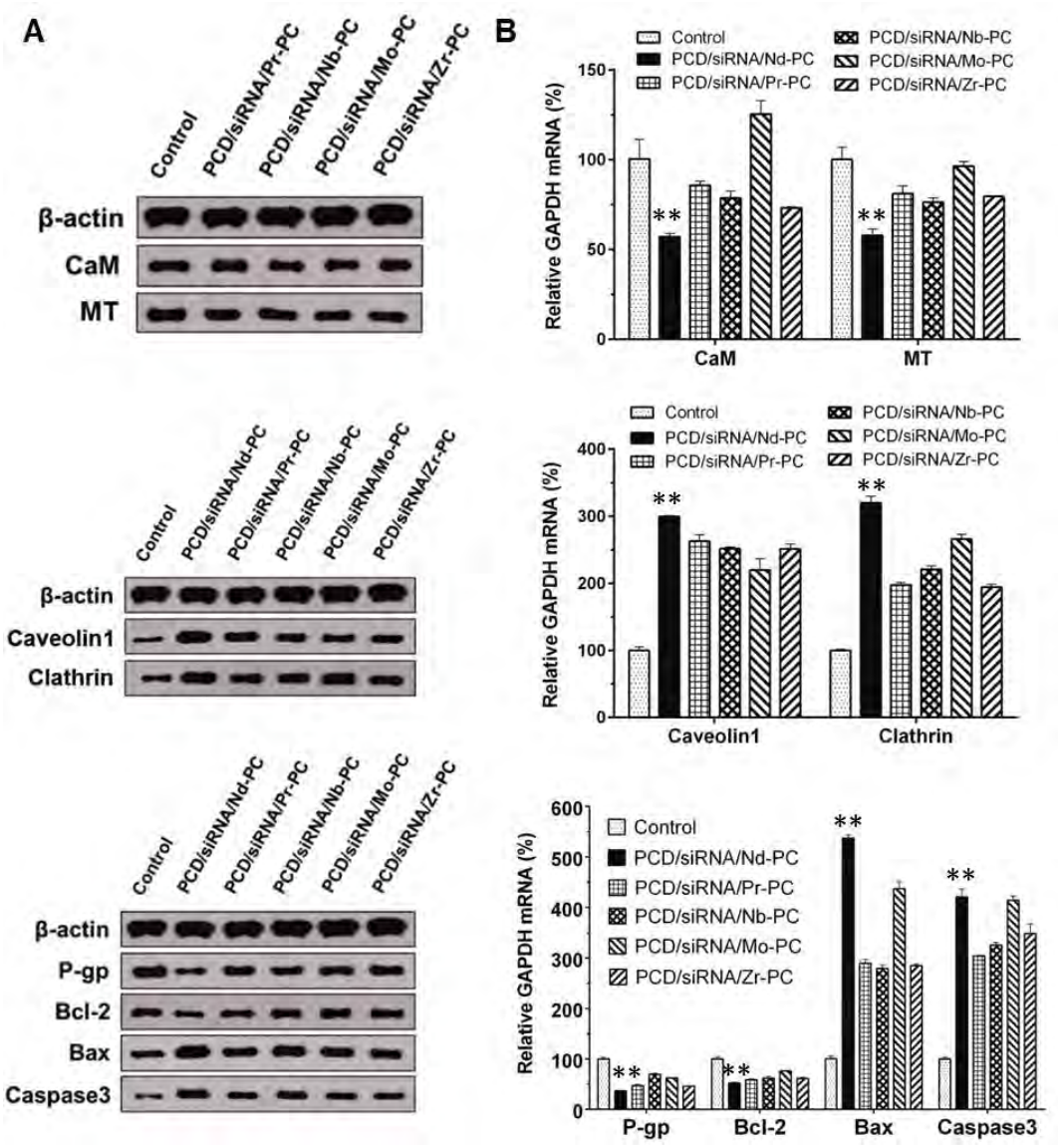

Fig. S15. (A) *In vitro* representative protein expression analyzed by western blot and (B) corresponding mRNA levels analyzed by RT-PCR in MCF-7/ADR cells mediated by PCD/siRNA/Nd-PC and other metal-functionalized nanoparticles. *P<0.05 and **P<0.01, PCD/siRNA/Nd-PC vs (PCD/siRNA/Pr-PC, PCD/siRNA/Nb-PC, PCD/siRNA/Mo-PC, PCD/siRNA/Zr-PC), except PCD/siRNA/Nd-PC vs PCD/siRNA/Mo-PC for Caspase3. The quantitative data represent mean ± SD (n = 3).

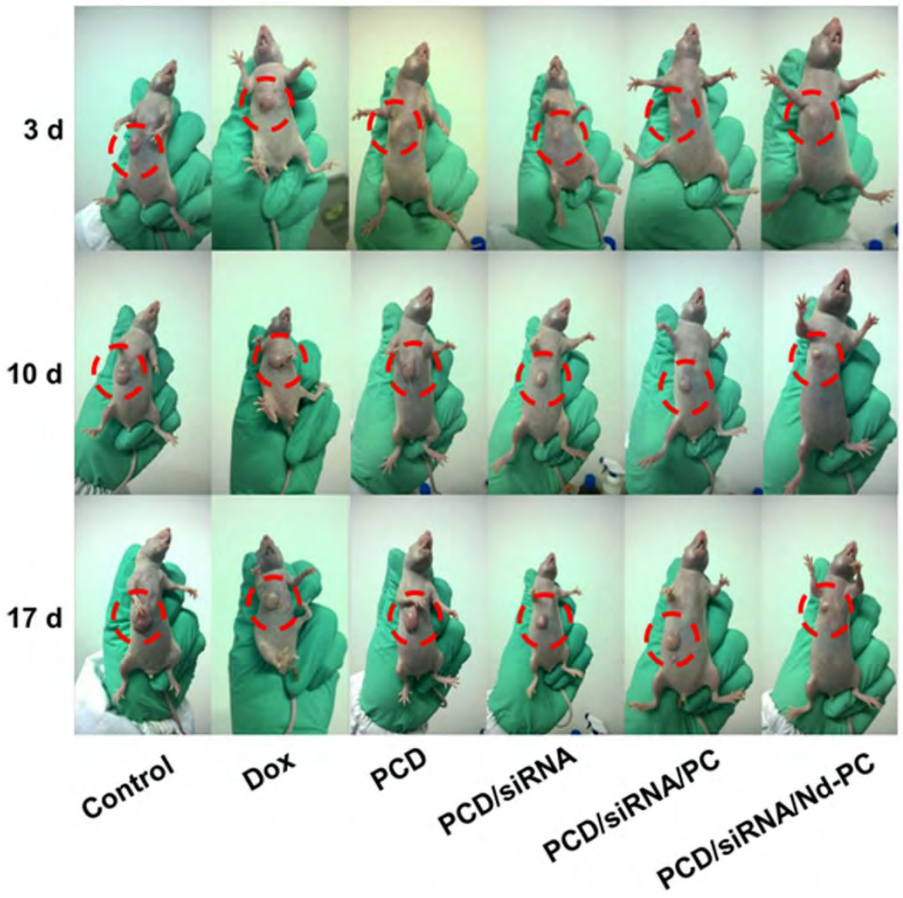

Fig. S16. Images of the tumor-bearing mice treated with various formulations for 3, 10, and 17 days.

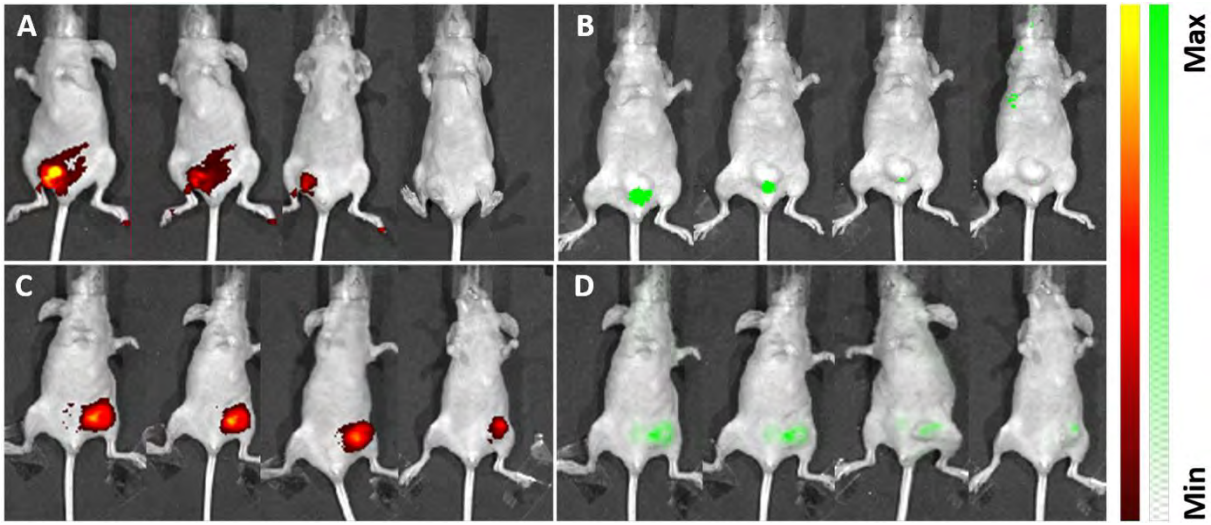

Fig. S17. In vivo fluorescence imaging of tumor-bearing mouse injected intratumorally of (A) free Dox, (B) FAM-siRNA, and (C, D) PCD/FAM-siRNA/Nd-PC for 1, 3, 6, and 12 h (from left to right).

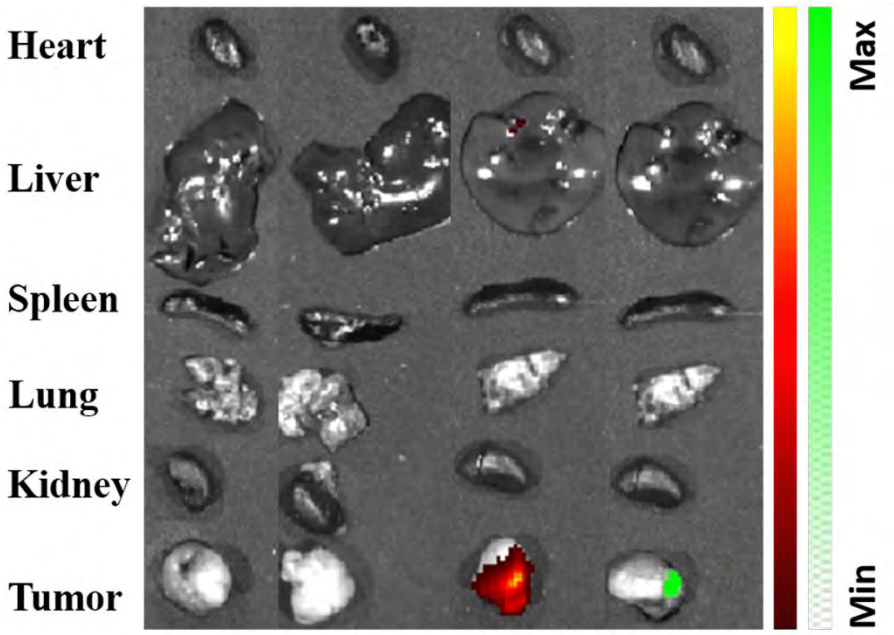

Fig. S18. The ex vivo images of tumors and organs of tumor-bearing mice sacrificed at 12 h after injected intratumorally with (left) free Dox, (middle) FAM-siRNA, and (the right two) PCD/FAM-siRNA/Nd-PC.

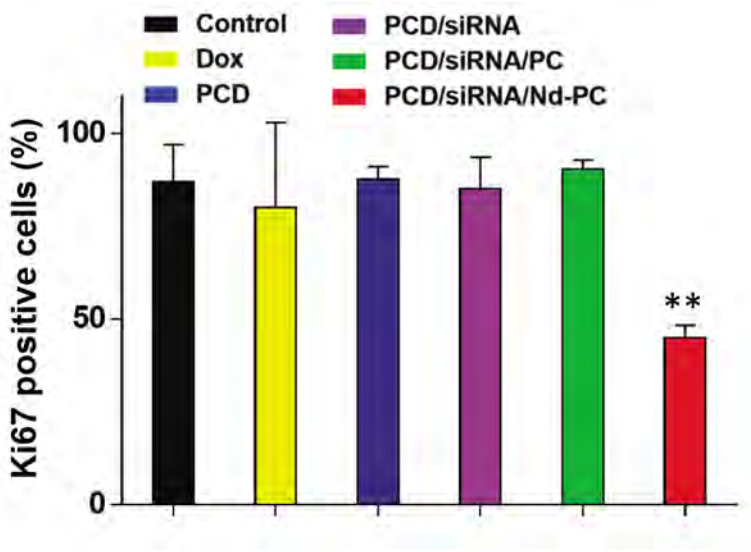

Fig. S19. Relative Ki67 positive cells after delivery of PCD/siRNA/Nd-PC or other formulations *in vivo*. **P<0.01, PCD/siRNA/PC vs PCD/siRNA/Nd-PC. The quantitative data represent mean ± SD (n = 3).

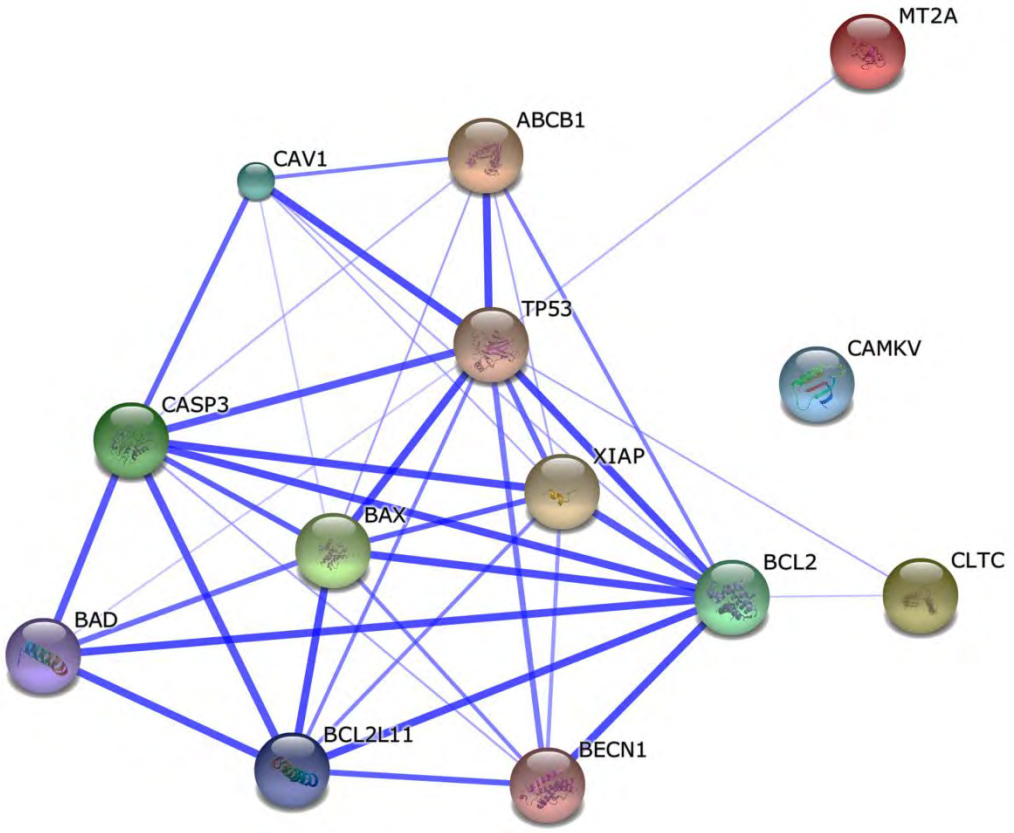

Fig. S20. Protein network analysis of the regulated proteins mediated by PCD/siRNA/Nd-PC. The relationships of 8 regulated proteins CaM (CAMKV), MT (MT2A), Caveolin1 (CAV1), Clathrin (CLTC), P-gp (ABCB1), Bcl-2 (BCL 2), Bax (BAX), and Caspase3 (CASP3), out of 13 relevant proteins are investigated. Thicker lines represent strong association and thinner lines represent weak association.

Table S1. Primers used in real-time PCR of selected gene transcripts.

Gene	Primer Sequences
Calmodulin (CaM)	Sense primer: 5- TGTCAGGCTGTCACTGTTCA -3
	Antisense primer: 5- GCTCCAAGTCATGGTTCAGA -3
Metallothionein (MT)	Sense primer: 5'- CTCAACTTCTTGCTTGGGATC -3'
	Antisense primer: 5'- AATGGGTCAGGGTTGTATGG -3'
Caveolin1	Sense primer: 5- TCTGCCTCTCCAAATATCCC -3
	Antisense primer: 5- TTCCTGGCTTCTCTTCACCT -3
Clathrin	Sense primer: 5- CAGCAAACATTGGCTTCAGT -3
	Antisense primer: 5- TCTGCTGAAATTGGTCTTCG -3
P-glycoprotein (P-gp)	Sense primer: 5- AAGGCATTTACTTCAAACTTGTCA -3
	Antisense primer: 5- TGGATTCATCAGCTGCATTTT -3
Bcl-2	Sense primer: 5- ATCCAGGATAACGGAGGC -3
	Antisense primer: 5- CAGCCAGGAGAAATCAAAC -3
Bax	Sense primer: 5- GACCCGGTGCCTCAGGATGC -3
	Antisense primer: 5- GTCTGTGTCCACGGCGGCAA -3
Caspase3	Sense primer: 5- TAAATGAATGGGCTGAGCTG -3
	Antisense primer: 5- ATGGAGAAATGGGCTGTAGG -3
GAPDH	Sense primer: 5- CATCTTCTTTTGCGTCGCCA -3
	Antisense primer: 5- TTAAAAGCAGCCCTGGTGACC -3

Table S2. Concentrations of Nd, Pr, Zr, Mo, and Nb in Nd-PC, Pr-PC, Zr-PC, Mo-PC, and Nb-PC determined by ICP-OES. The quantitative data represent mean ± SD (n = 3).

	Total element [wt‰]	Free-state element [wt‰]	Coordinated element [wt‰]
Nd	0.9896 ± 0.0147	0.2398 ± 0.0037	0.7498
Pr	0.6588 ± 0.0324	0.1570 ± 0.0049	0.5018
Zr	0.3348 ± 0.0150	0.0582 ± 0.0013	0.2766
Mo	0.3536 ± 0.0121	0.3260 ± 0.0180	0.0276
Nb	0.1130 ± 0.0027	0.0597 ± 0.0032	0.0533